ANL-80-115
Part I

ANL-80-115
Part I

RADIOLOGICAL AND ENVIRONMENTAL RESEARCH DIVISION ANNUAL REPORT

Fundamental Molecular Physics and Chemistry

October 1979—September 1980

ARGONNE NATIONAL LABORATORY, ARGONNE, ILLINOIS

Prepared for the U. S. DEPARTMENT OF ENERGY
under Contract W-31-109-Eng-38

FOREWORD

This is the tenth Annual Report on our Section's work on the physics and chemistry of atoms, ions, and molecules — especially their interactions with external agents such as photons and electrons. As will be seen, this year has been one of vigorous activity.

Our main programs address themselves to some basic-science problems fundamental to the needs of DOE and other government agencies. For instance, the cross-section data for photoabsorption and photoionization, as well as for electron collisions, are indispensable to a sound modeling of the action of all ionizing radiations on matter, including biological substances. Further, the spectroscopic data for some molecules and clusters of molecules are crucial for the modeling of atmospheric chemistry of pollutants. Work in the above areas is supported by the Office of Health and Environmental Research, DOE.

Another program concerns atomic physics essential to fusion-energy technology. This program is being supported by the Office of Magnetic Fusion.

More recently, new programs have been initiated in molecular spectroscopy by the use of lasers as well as synchrotron radiation. Some of the work in these areas is conducted under financial support from the Office of Naval Research, Department of Defense, and other work is carried out in collaboration with the National Bureau of Standards, U.S. Department of Commerce. We take this opportunity to thank these agencies for their generous help which has made possible a great expansion of the scope of our work.

The articles in the present report are loosely arranged according to the subject matter they treat. Papers 1-20 concern photoabsorption and its consequences. Note paper 20, which describes a new activity, i.e., studies on multiphoton processes. Papers 21-28 concern electron collisions with atoms and molecules and closely related topics. Papers 29-34 pertain to theoretical atomic physics related to radiation physics, and papers 35-37 treat fusion-related atomic physics.

We are pleased to announce that J. L. Dehmer and Y.-K. Kim have been elected to the Fellowship of The American Physical Society for their significant

contributions to electron and atomic physics. In addition, we have enjoyed considerable recognition in the international physics community outside the Laboratory in several respects. First, P. M. Dehmer serves as Secretary-Treasurer of the Division of Electronic and Atomic Physics of The American Physical Society and is also a member of the Publication Committee. Second, David Spence is spending the academic year 1980-1981 at the Joint Institute for Laboratory Astrophysics of the University of Colorado and of the National Bureau of Standards as a Visiting Fellow. Third, M. Inokuti was awarded a fellowship from NORDITA (Nordisk Institut for Teorisk Atomfysik), Copenhagen, Denmark, to serve from April to July 1980 as a Visiting Professor at the Institute of Physics, Odense University. Finally, M. Inokuti has served as a Councilor for the Radiation Research Society, has worked as a member of the Physics Panel for the Department of Health, Education, and Welfare study on the Agenda for Research into the Biological Effects of Ionizing Radiations (the final report of this work has recently been issued by the National Institutes of Health) and continues to work as Vice-Chairman of the Committee on Stopping Power for the International Commission on Radiation Units and Measurements.

Mitio Inokuti

TABLE OF CONTENTS

Fundamental Molecular Physics and Chemistry

PHOTOIONIZATION AND PHOTOFRAGMENTATION OF SMALL CLUSTERS OF RARE-GAS ATOMS

P. M. Dehmer and S. T. Pratt*

The relative photoionization cross sections for Ar_3, Ar_4, Ar_5, and Ar_6 have been measured from threshold to 700 Å at high nozzle stagnation pressures. Under these nozzle consitions very heavy Ar clusters are formed, and their fragmentation is shown to dominate the photoionization efficiency curves of the lighter clusters. The spectrum of the trimer changes dramatically as a function of nozzle stagnation pressure, clearly demonstrating the effects of fragmentation.

The relative photoionization cross sections of small rare-gas clusters have been obtained using a photoionization mass spectrometer which incorporates a free supersonic molecular beam source. A brief description of the apparatus has been given previously,[1] and the system will be described in more detail in a future article. The main components of the apparatus are a helium Hopfield continuum light source, a 1-meter near-normal incidence monochromator equipped with a 1200 line/mm MgF_2-coated Al grating, an ion focussing lens system, and a differentially-pumped quadrupole mass filter. The wavelength selected photons are crossed by a molecular beam from a free supersonic expansion. In the experiments described here, pure argon was expanded through an orifice which was typically 10 to 12 μm in diameter.

Figure 1 shows a plot of the pressure dependence of the Ar_n^+ ion signals for n = 2 to 6 measured at a resolution of 0.45 Å and at a wavelength of 772.5 Å. At this wavelength, which is above the $Ar^+ {}^2P_{1/2}$ ionization limit, neither the atom spectrum nor any cluster spectrum exhibits sharp structure. It has been observed in previous studies[2-4] and can be seen in Figure 1, that the dimer can be prepared in the beam over a wide range of pressures where the presence of larger clusters is not detectable. Preparation of a beam containing only monomer, dimer, and trimer is much more difficult, and perhaps impossible, since the tetramer and large clusters are observed at a stagnation pressure only slightly higher than

*Thesis Parts Participant. Permanent address: Department of Chemistry, Yale University, New Haven, Connecticut 06511.

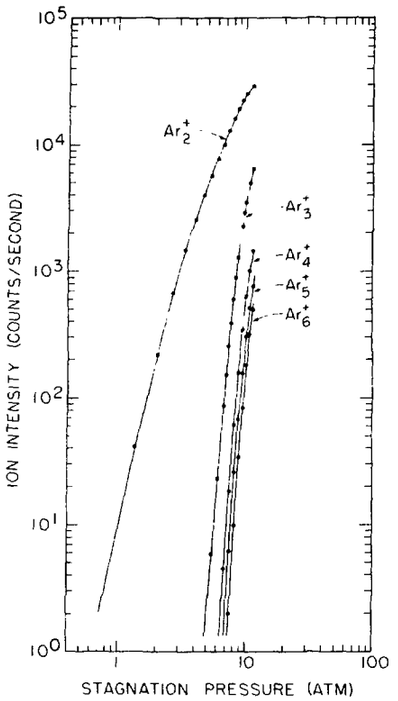

FIG. 1.--Pressure dependence of the Ar_n^+ ion signal measured at 772.5 Å using a 12-1/2 μm jet.

that at which the trimer is first observed.

Figure 2 shows the present dependence of the trimer spectrum. The nozzle conditions were identical to those of Figure 1, and the wavelength resolution was 0.45 Å. There is a significant difference in the cluster populations of the high and low pressure beams. At the highest pressure shown in Figure 2, the tetramer, pentamer, and hexamer ion signals are 22%, 12%, and 8% of the trimer ion signal, respectively (at 772.5 Å). At the lowest pressure the tetramer ion signal is approximately 4% of the trimer ion signal with no detectable heavier clusters. There is a striking difference in the trimer photoionization efficiency curves for the different nozzle conditions. The lowest pressure spectrum exhibits a sharp step at threshold followed by several more steps which lead to a maximum at 805 Å, while in the highest pressure spectrum this structure is almost completely washed out with the photoionization efficiency curve rising smoothly to a maximum at 750 Å. The significant increase in relative intensity at shorter wavelengths for the high pressure runs shows that fragmentation does occur and is the dominant mechanism for trimer ion production at higher energies. Similarly,

the high pressure photoionization efficiency curves of the heavier clusters will also be dominated by fragmentation and would be expected to have nearly identical shapes. This is, in fact, the case. Figure 3 shows the spectra of several clusters (n = 3 to 6) of Ar taken at a stagnation pressure of 11.55 atm and with a jet that was approximately 10% larger in diameter than that used for the previous runs. This difference in nozzle diameter resulted in a slightly different shape for the trimer spectrum from that shown in Figure 2 taken at the same stagnation pressure. The difference in shape is attributable to the production and subsequent fragmentation of heavier clusters.

The general appearance of the four spectra in Figure 3 is remarkably similar. All of the curves show a broad maximum peaking at 750 Å (16.53 eV), which probably reflects a maximum in the absorption cross section of larger clusters. Some evidence for such a maximum is found in the reflectance spectrum of solid argon, which has such a feature at 16.05 eV.[5] This same feature is seen at 16.5 eV in electron energy loss spectra of solid argon[6] with the energy difference being attributed to sample preparation.

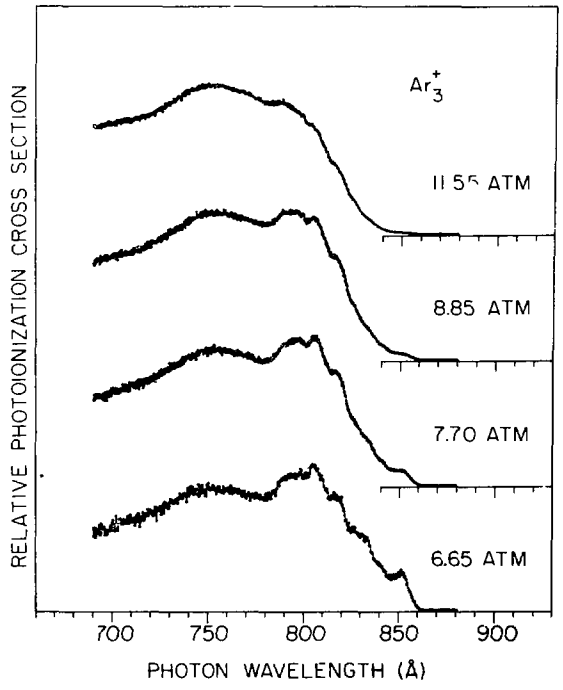

FIG. 2.--Relative photoionization cross sections for Ar_3 measured at a wavelength resolution of 0.45 Å using a 12-1/2 μm jet. The nozzle stagnation pressures are indicated on the figure.

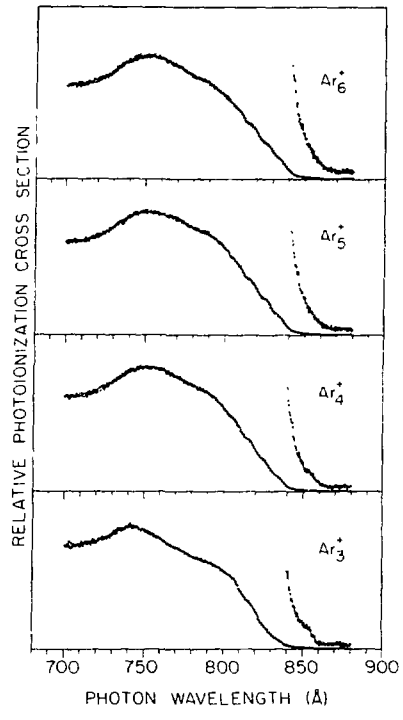

FIG. 3.--Relative photoionization cross sections for Ar_3 to Ar_6 measured at a wavelength resolution of 0.45 Å using a 12-1/2 μm jet. The nozzle stagnation pressure was 11.55 atm for all the runs.

We are now working to understand both the low pressure trimer spectrum (which is representative of the true trimer spectrum) and the high pressure trimer and heavier spectra (which are representative of the spectra of all of the heavier clusters).

References

1. P. M. Dehmer and E. D. Poliakoff, Chem. Phys. Lett. 77, 326 (1981).
2. A. van Deursen, A. van Lumig, and J. Reuss, Int. J. Mass Spectrom. Ion Phys. 18, 129 (1975).
3. D. Golomb, R. E. Good, and R. F. Brown, J. Chem. Phys. 52, 1545 (1970).
4. D. Golomb, R. E. Good, A. B. Bailey, M. R. Busby, and R. Dawbårn, J. Chem. Phys. 57, 3844 (1972).
5. B. Sonntag, Rare Gas Solids, Vol. II, M. L. Klein and J. A. Venables, Eds., Academic Press, London, pp. 1020-1117 (1977).
6. J. A. Nuttall, T. E. Gallon, M. G. Devey, and J.A.D. Matthew, J. Phys. C 8, 445 (1975).

APPEARANCE POTENTIALS OF Ar_n^+ CLUSTER IONS

P. M. Dehmer and S. T. Pratt*

The photoionization appearance potentials for Ar_2^+ and Ar_3^+ were determined at a resolution of 0.45 Å using several different nozzle stagnation pressures in order to investigate the effects of fragmentation on the threshold. The appearance potentials for Ar_4^+, Ar_5^+, and Ar_6^+ were also determined.

As is shown by Eq. 1 below, accurate values of the adiabatic ionization potential (IP) of the Ar_n and Ar_{n-1} clusters are required to calculate the dissociation energy of the Ar_n^+ molecular ion.

$$D_0(Ar_{n-1}^+ - Ar) = IP(Ar_{n-1}) + D_0(Ar_n) - IP(Ar_n) \quad . \tag{1}$$

A fundamental problem for the smaller rare gas clusters is that, because of the large change in geometry upon ionization, the Franck-Condon factor for ionization to the vibrational ground state is extremely small. In fact, for the argon dimer the Franck-Condon factor is negligible for approximately 0.8 eV above the adiabatic IP.[1] Although the Franck-Condon factor between the neutral and ionic states of the trimer may be better, there is still a large geometry change, and direct ionization will be insignificant near the adiabatic IP.[2] Ionization is observed, however, in the threshold region, but for the dimer and trimer (and probably many of the heavier clusters), this ionization is due solely to autoionization. Thus, the adiabatic IP will be observed only if there is a high density of autoionizing molecular Rydberg states in the threshold region.

We have attempted to determine whether the adiabatic IPs of Ar_2 and Ar_3 are actually observed by making a careful study of the threshold regions of these clusters at two different pressures. Assuming that the dissociation energy of a neutral cluster Ar_n into Ar_{n-1} + Ar is equal to the dimer dissociation energy of 12 meV,[3] then dissociative ionization of Ar_n to form Ar_{n-1}^+ + Ar will have a threshold 12 meV above the Ar_{n-1} adiabatic ionization threshold (e.g., Ar_2^+ will

*Thesis Parts Participant. Permanent address: Department of Chemistry, Yale University, New Haven, Connecticut 06511.

be formed via dissociative ionization of Ar_3 at 12 meV, or approximately 0.7 Å, above the Ar_2 adiabatic IP). Thus, a comparison of the appearance potential of Ar_2 obtained with a low pressure beam (containing only monomer and dimer) and with a high pressure beam (containing a mixture of heavy clusters) is very instructive. If the appearance potential is invariant with nozzle stagnation pressures, this is strong evidence that the appearance potential is actually the adiabatic ionization potential.

Figure 1 shows the Ar_2 threshold region taken at a wavelength resolution of 0.45 Å and at stagnation pressures of 3.06 and 10.18 atm. The counting rate at 848 Å was approximately a factor of three greater in the high pressure run. The threshold region of the high pressure run rises more steeply than that of the low pressure run, but in both cases the threshold is at 855.0 ± 1.5 Å, lower than our previously reported value,[4] and reflects the extremely conservative estimate of the magnitude of the collisional ionization. A careful inspection of Figure 1 shows that the structure in the two runs is identical, but that in the high pressure run it is superimposed on a structureless background. This background is due to fragmentation of larger clusters. The fact that the threshold does not shift as a result of fragmentation supports the hypothesis that the adiabatic IP actually is observed.

Figure 2 shows the Ar_3 threshold region taken at a wavelength resolution of 0.45 Å and stagnation pressures of 5.15 and 11.55 atm. These stagnation pressures yielded 15 and 7.5×10^3 ion counts per second, respectively, at 800 Å. From expanded versions of Figure 2 the threshold was determined to be 865.0 ± 1.5 Å. There is no apparent shift in the appearance potential (AP) with pressure; however, the statistics are poorer than those of the dimer runs.

Assuming that the appearance potentials for Ar_2^+ and Ar_3^+ are equal to the adiabatic ionization potentials, and using a value of 12 meV for $D_0(Ar_3)$, the dissociation energy of Ar_3^+ is calculated to be 0.18 ± 0.05 eV. Turner and Conway[5] and Fehsenfeld et al.[6] have obtained values of the dissociation energy of Ar_3^+ of 0.219 ± 0.005 eV and 0.217 eV, respectively, by studying the temperature dependence of the reaction $Ar_2^+ + Ar \rightarrow Ar_3^+$ using the flow tube techniques.

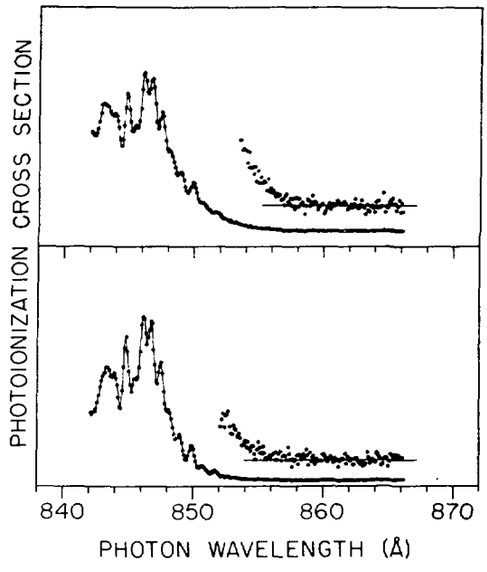

FIG. 1.--Relative photoionization cross sections for Ar_2^+ near threshold taken at a wavelength resolution of 0.45 Å using 12.5 μm supersonic molecular beam source. The stagnation pressures for the two runs were 3.06 atm (lower frame) and 10.18 atm (upper frame).

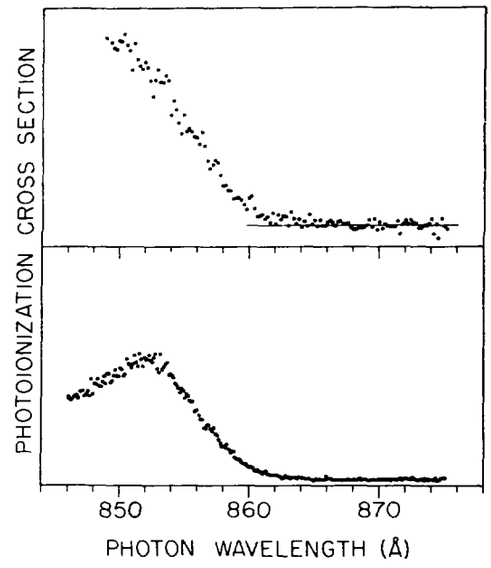

FIG. 2.--Relative photoionization cross section for Ar_3^+ near threshold taken at a wavelength resolution of 0.45 Å using a 12.5 μm supersonic molecular beam source. The stagnation pressures for the two runs were 5.15 atm (lower frame) and 11.55 atm (upper frame).

Two recent theoretical calculations give values of the Ar_3^+ dissociation energy intermediate between the values obtained from the drift tube experiments and those obtained from the present photoionization experiments. Michels et al.[7] obtained a value of 0.17 eV based on a triangular ionic state, while Wadt[8] obtained a value of 0.18 eV from a more accurate ab initio calculation which predicted a linear ionic state.

The appearance potentials of the heavier cluster ions Ar_4^+, Ar_5^+, and Ar_6^+ have also been measured. To a first approximation, they all have a value of 868.0 ± 2.0 Å; however, the cross sections in this region are extremely weak, and in all cases, the ionization onset is gradual. We are currently investigating these thresholds in more detail.

References

1. P. M. Dehmer and J. L. Dehmer, J. Chem. Phys. 69, 125 (1978).
2. E. D. Poliakoff, P. M. Dehmer, J. L. Dehmer, and R. Stockbauer, submitted for publication.
3. R. J. LeRoy, J. Chem. Phys. 57, 573 (1972).
4. P. M. Dehmer and E. D. Poliakoff, Chem. Phys. Lett. 77, 326 (1981).
5. D. L. Turner and D. C. Conway, J. Chem. Phys. 71, 1899 (1979).
6. F. C. Fehsenfeld, T. J. Brown, and D. L. Albritton, Bull. Am. Phys. Soc. 24, 124 (1979).
7. H. H. Michels, R. H. Hobbs, and L. A. Wright, Appl. Phys. Lett. 35, 153 (1979).
8. W. R. Wadt, Appl. Phys. Lett., in press.

AUTOIONIZATION OF Ar_2 RYDBERG STATES FOLLOWING PHOTOABSORPTION

P. M. Dehmer and E. D. Poliakoff*

The relative photoionization cross section of Ar_2 was measured in the wavelength region 775 to 860 Å at a resolution of 0.28 Å. Portions of the spectrum were taken at higher resolution. Figure 1 shows a small portion of the spectrum taken at a resolution of 0.07 Å which encompasses the first prominent structure above the ionization threshold. Autoionization dominates this region of the spectrum and there is no contribution from direct ionization.[1] A comparison of the ionization spectrum and the high resolution liquid nitrogen temperature absorption spectrum obtained by Tanaka and Yoshino[2,3] reveals significant differences in the intensities of some of the peaks. For example, the very weak peaks at $\sim$ 119600 cm^{-1} in the ionization spectrum are among the most intense peaks in this region in the absorption spectrum. This suggests that predissociation and/or fluorescence may be alternate decay paths for these molecular states.

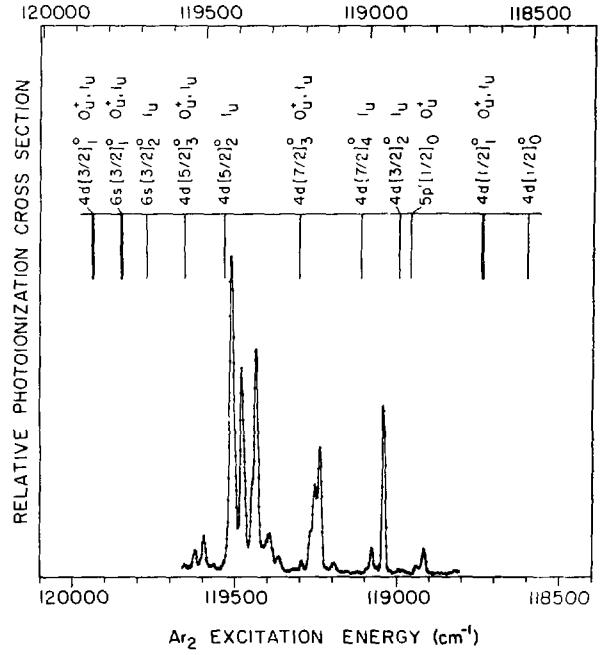

FIG. 1.--Relative photoionization cross section for Ar_2^+ (Ar_2) near the ionization threshold. The atomic energy levels are also shown in the figure, with those that are optically allowed indicated by heavy lines. Optically allowed molecular states dissociating to these atomic limits are indicated. The atomic transitions are shifted in energy with respect to the molecular transitions by an amount equal to D_0 of the ground state; this places the atomic and the molecular transitions on the same energy scale assuming that all of the molecular transitions originate in v" =0 of the ground state.

---

*NSF Postdoctoral Fellow, September 1979-August 1980.

Incipient vibrational structure observed in many of the bands is the basis for tentative Rydberg state assignments. Many of these Rydberg states are expected to be members of series converging to excited states of the Ar_2^+ molecular ion. The most striking feature of the spectrum in the region above the ionization threshold is the lack of regular structure, indicating that curve crossings and perturbations severely affect the potential energy curves.

References

1. P. M. Dehmer and J. L. Dehmer, J. Chem. Phys. 69, 125 (1978).
2. Y. Tanaka and K. Yoshino, J. Chem. Phys. 53, 2012 (1970).
3. Y. Tanaka, private communication.

PHOTOIONIZATION OF THE Kr_2 DIMER

S. T. Pratt* and P. M. Dehmer

Preliminary results on the photoionization of the Kr_2 van der Waals molecule are presented. Autoionization structure is observed throughout the region studied, and above the $^2P_{3/2}$ atomic Kr limit the Kr_2^+ structure strongly resembles that of Kr^+ but is shifted to longer wavelengths, yielding information on the dissociation energies of these excited states.

The relative photoionization cross section of the Kr_2 dimer was determined at a resolution of 0.15 Å (FWHM) in the wavelength region 900 to 970 Å with a photoionization mass spectrometer which incorporated a supersonic molecular beam source for the production of the Kr_2 van der Waals molecule. The unskimmed molecular beam was photoionized using monochromatized light from the helium Hopfield continuum, and the resulting photoions were mass analyzed with a quadrupole mass filter.[1,2]

Figure 1 shows the Kr_2 spectrum obtained with a 25 μm orifice and a stagnation pressure of 2.44 atm. At this stagnation pressure there is very little trimer in the beam. Spectra taken at higher stagnation pressures exhibit the same structure superimposed on a background continuum, which is due to fragmentation of larger clusters. The general features of the fragmentation process have been discussed previously for Ar_2 and Ar_3.[3] Also shown in Figure 1 is the spectrum of atomic krypton obtained using the same orifice and a stagnation pressure of 0.29 atm.

The equilibrium bond distance is 4.007 Å[4] in Kr_2 neutral and 2.79 Å[5,6] in the Kr_2^+ ion. Because of this large difference in equilibrium geometry, direct ionization is negligible until approximately 920 Å,[5] and autoionization accounts for all of the observed structure, with the exception of some readily identifiable chemi-ionization lines. Because there is no direct ionization near the lowest threshold, we must rely on a high density of autoionizing states in this region

*Thesis Parts Participant. Permanent address: Department of Chemistry, Yale University, New Haven, Connecticut 06511.

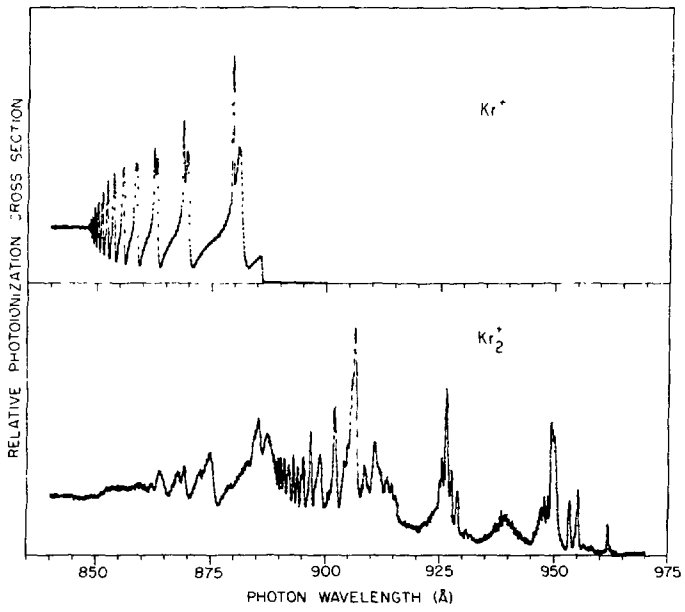

FIG. 1.--Relative photoionization cross sections for Kr and Kr_2 from a supersonic nozzle with a 25 μm diameter orifice and stagnation pressures of 0.29 and 2.44 atm, respectively, both taken with 0.15 Å resolution.

to observe the adiabatic ionization potential. The appearance potential, which we equate with the adiabatic IP is 963.85 ± 0.15 Å. Using 16[5] meV as the dissociation energy D_0 of Kr_2 neutral, and 885.63 Å as the IP of atomic Kr,[7] we found the dissociation energy D_0 of Kr_2^+ to be 1.152 ± 0.002 eV. This is in excellent agreement with the results of Ng et al.[8] who measured the photoionization cross section of Kr_2 at low resolution using a skimmed supersonic beam. As in the case of the Ar_2 dimer, this indicates that collisional ionization is not a serious problem when free, unskimmed jets are used to determine accurate adiabatic IPs for van der Waals molecules. In addition, the high sensitivity due to increased number density in the free jet makes it an extremely useful technique.

There are six electronic states of the Kr_2^+ ion in the wavelength region of Figure 1.[9] The ground state and the first three excited states of Kr_2^+ dissociate to a ground state atom and a $^2P_{3/2}$ ion; in the nomenclature appropriate for small internuclear distances these states are labelled A $^2\Sigma^+_{1/2u}$, B $^2\Pi_{3/2g}$, C $^2\Pi_{3/2u}$, and B $^2\Pi_{1/2g}$ in order of increasing energy.[9] The adiabatic thresholds of the A $^2\Sigma^+_{1/2u}$ and B $^2\Pi_{3/2g}$ states are 963.85 and 895.2 Å,[5] respectively. The C $^2\Pi_{3/2u}$ and B $^2\Pi_{1/2g}$ states are either very weakly bound or purely repulsive in the Franck-Condon region,[5,6] and their thresholds are very near the $^2P_{3/2}$ atomic IP. The next two excited states are labelled C $^2\Pi_{1/2u}$ and D $^2\Sigma^+_{1/2g}$ and

dissociate to a ground state atom and a $^2P_{1/2}$ ion.[9] The adiabatic IP of the C $^2\Pi_{1/2u}$ state is 852.7 Å,[5] and the D state is probably repulsive.[6] Thus, from threshold to 895.2 Å there are autoionizing Rydberg series converging to the five electronically excited limits, as well as Rydberg states with vibrationally excited A state cores. As in the case of Ar_2^+,[1] the occurrence of curve crossings and perturbations between the large number of states in this region removes nearly all of the regularity in the observed structure. We are now in the process of analyzing several of the low-lying bands in greater detail.

The region between about 900 Å and the $^2P_{3/2}$ atomic IP at 885.6 Å is very complicated owing to the large number of autoionizing molecular states and the chemi-ionizing atomic states converging to the $^2P_{3/2}$ limit.

Above the $^2P_{3/2}$ atomic IP there are only two atomic Rydberg series, ns' and nd', and the Kr_2 spectrum becomes noticeably simpler. Even so, following standard coupling rules,[10] it is found that the combination of $Kr(^1S_0) + Kr^*(ns')$ gives rise to two optically allowed molecular states and that $Kr(^1S_0) + Kr^*(nd')$ gives rise to six allowed states, yielding a total of eight optically allowed series. Because the D $^2\Sigma^+_{1/2g}$ state is repulsive,[5,6] molecular states converging to this limit should be shifted approximately 16 meV[5] (the Kr_2 neutral dissociation energy D_0) to the blue of the atomic Rydberg states. Most of the dimer peaks are shifted to the red of the atomic structure and thus appear to be in Rydberg series converging to the C $^2\Pi_{1/2u}$ limit. Although there are very few trends in the quantum defects of these states, preliminary analysis indicates that the peaks at 885.4, 874.7, and 869.3 Å are part of a Rydberg series converging to the C $^2\Pi_{1/2u}$ limit. The dissociation energies calculated for these molecular states increase monotonically in the series toward the ionic dissociation energy, and the quantum defects are relatively constant. Further analysis, as well as experiments in the analogous region in Xe_2, will lead to a better understanding of these states.

References

1. P. M. Dehmer and E. D. Poliakoff, Chem. Phys. Lett. 77, 326 (1981).
2. P. M. Dehmer, to be published.

3. P. M. Dehmer and S. T. Pratt, to be published.
4. J. A. Barker, R. O. Watts, J. K. Lee, T. P. Schafer, and Y. T. Lee, J. Chem. Phys. 61, 3081 (1974).
5. P. M. Dehmer and J. L. Dehmer, J. Chem. Phys. 69, 125 (1978).
6. W. R. Wadt, J. Chem. Phys. 68, 402 (1978).
7. K. Yoshino and Y. Tanaka, J. Opt. Soc. Am. 49, 159 (1979).
8. C. Y. Ng, D. J. Trevor, B. H. Mahan, and Y. T. Lee, J. Chem. Phys. 66, 446 (1977).
9. R. S. Mulliken, J. Chem. Phys. 52, 5170 (1970).
10. G. Herzberg, Spectra of Diatomic Molecules, Von Nostrand, Princeton, pp. 319-320 (1950).

DESIGN OF A PHOTOELECTRON-PHOTOION COINCIDENCE SPECTROMETER FOR STUDIES OF GAS-PHASE CLUSTER SPECIES*

E. D. Poliakoff, P. M. Dehmer, J. L. Dehmer, and Roger Stockbauer†

Clusters of atoms have properties qualitatively different from those of either free atoms or macroscopic solids. There is great interest in the microscopic physical and chemical properties of small clusters because they are prototype systems for the study of catalysis and aerosol formation. Among the possible experimental probes of clusters, photoelectron spectroscopy is particularly desirable for several reasons. The photoelectron spectrum of a cluster yields information directly on the electronic properties of the cluster and cluster ion, e.g., ionization potentials and relative transition strengths. Indirectly, structural information is obtained by correlating peak shapes with Frank-Condon envelopes. Furthermore, there is a wealth of photoelectron spectra for free atoms and solids, i.e., the limits of cluster behavior. Unfortunately, conventional photoelectron spectroscopy of clusters is impractical because methods of cluster production result in a broad distribution of n-mer sizes, leading to severe difficulties in selectively probing a particular cluster. In this report we describe an instrument that detects the ion mass in coincidence with the photoelectron kinetic energy, and thus surmounts the primary obstacle which prevents acquisition of unambiguous, mass-specific photoelectron spectra.

The experimental apparatus consists of a 2-in mean radius electron spectrometer,[1] a time-of-flight mass spectrometer, a dc discharge resonance lamp (He I, 21.21 eV), and a free-jet supersonic molecular beam source;[2] see Figure 1 for the experimental schematic. For the present measurements, electrons ejected at 90° with respect to the radiation propagation vector passed through a 0.080 in diameter slit and were analyzed at 5 eV pass energy, resulting in 110 meV electron energy resolution. The mass spectrometer consists of ten stack plates, followed by a drift tube, two biasing grids, and a

*Summary of a paper being prepared for publication.

†National Bureau of Standards, Washington, D.C. 20234.

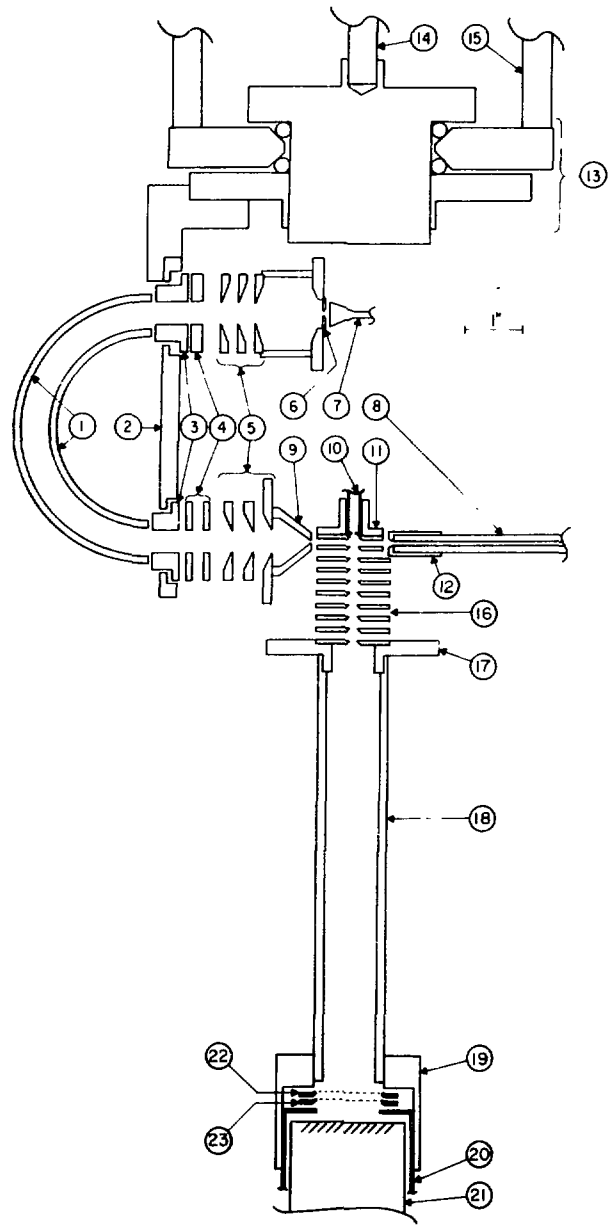

FIG. 1.--Schematic diagram of the experimental apparatus. The main components are:

(1) Concentric hemispheres
(2) Mounting plate for hemispheres and entrance and exit lenses
(3) Herzog lenses
(4) Deflector plates
(5) Three-aperture "zoom" lenses
(6) Exit aperture
(7) Channeltron detector
(8) 2-mm (i.d.) capillary leading to lamp (not shown)
(9) Entrance aperture
(10) Supersonic gas jet
(11) Gas jet holder
(12) Shield and holder for capillary tube
(13) Sapphire ball bearing
(14) Drive shaft
(15) Mounting rods
(16) Ion acceleration stack plates
(17) Holder for stack plates and drift tube
(18) Drift tube
(19) Drift tube-detector mounting bracket
(20) μ-metal detector housing
(21) "Venetian blind" electron multiplier
(22) Drift tube potential grid
(23) Retarding grid

detector (venetian blind electron multiplier). The gas beam intersects the VUV radiation between the first two stack plates. The first five plates are quiescently grounded and receive a voltage pulse to extract the ion upon detection of an electron. The whole system is interfaced to a microcomputer via a CAMAC crate. Sample Xe cluster spectra (see next report) require data accumulation of three hours for a particular mass and electron energy. The false coincidences are measured by generating a random "electron" pulse and observing the resulting mass spectral intensities. For the present measurements, a 2.5-μm diameter nozzle is used. The electronics which drive this apparatus will be discussed in a forthcoming article.[3] Experimental results are given in the following report.

References

1. J. L. Dehmer and D. Dill, Phys. Rev. A 18, 164 (1978).
2. P. M. Dehmer and J. L. Dehmer, J. Chem. Phys. 69, 125 (1978); 68, 3462 (1978).
3. E. D. Poliakoff, P. M. Dehmer, J. L. Dehmer, and Roger Stockbauer, to be published.

THE PHOTOELECTRON SPECTRUM OF Xe_3 BY THE PHOTOELECTRON-PHOTOION COINCIDENCE TECHNIQUE *

E. D. Poliakoff, P. M. Dehmer, J. L. Dehmer, and Roger Stockbauer†

Using the apparatus described in the previous report, we have obtained the first photoelectron-photoion coincidence spectrum of a single component, namely Xe_3, in a mixture of clusters. Thus we have selected the photoelectron spectrum of Xe_3 out of overlapping photoelectron spectra of Xe, Xe_2, Xe_3,... present in the beam. This measurement is the first step toward elucidation of the electronic structure changes occurring in the condensation of free atoms to form solids.

For comparison, the photoelectron-photoion coincidence spectrum of Xe_2^+ was also measured. Because the Xe_2 photoelectron spectrum has already been determined by a simpler method,[1] the dimer coincidence spectrum provides a check for experimental artifacts. Because the dimer spectrum is so markedly different from the trimer spectrum (as will be shown), the comparison demonstrates the value of the coincidence technique for selective studies of cluster species.

The stagnation pressure used to produce a beam of monomer plus dimer‡ was 1.51 atm; for a beam containing monomer, dimer, trimer, and very small amounts of higher n-mers, the stagnation pressure was 2.19 atm. Higher stagnation pressure spectra of trimer were recorded to ensure that fragmentation of higher n-mers did not significantly affect the Xe_3 results.[3]

Portions of the coincidence spectra of Xe_2 and Xe_3 are shown in Figure 1, revealing considerable differences.§ The vertical ionization potential (IP) shifts from

---

*Summary of an article published in J. Chem. Phys. 75, 1568 (1981).

†Surface Science Division, National Bureau of Standards, Washington, D.C. 20234.

‡Conditions can be obtained where only monomer and dimer are present. (See Refs. 1 and 2.

§It should be noted that states of Xe_3^+ that fragment will not be counted as coincidences and thus will not appear in the Xe_3 spectrum shown in Figure 1.

11.85 eV in Xe_2[1] to 11.47 ± 0.09 eV in Xe_3. The peak in the Xe_3 spectrum is also broader than the one in the Xe_2 spectrum. Several sources of broadening account for the width of this Xe_3 peak. First, the 1 eV region shown is predicted to contain vertical transitions to the four lowest ionic states of Xe_3^+,[4] some of which undoubtedly overlap because of the 110 meV electron energy resolution. Second, the neutral ground state geometry is triangular with internuclear separations of 4.36 Å,[5] while the ionic ground state is predicted to be linear with an internuclear separation of 3.47 Å.[6] Because of the extreme change in equilibrium geometry upon excitation to the ionic ground state, a broad Franck-Condon envelope is expected. Finally, the Xe_3 clusters formed in the supersonic expansion may be vibrationally excited, thus further contributing to the broadening.

The relationships that exist between the photoelectron appearance potentials and adiabatic IP's for Xe_2 and Xe_3 show the start of a trend. Although the adiabatic IP of Xe_3 has not been determined directly, it can be estimated from Eq. 1.

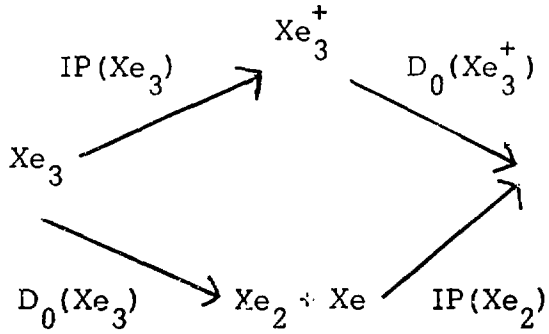

$$Xe_3 \xrightarrow{IP(Xe_3)} Xe_3^+ \xrightarrow{D_0(Xe_3^+)} Xe_2^+ + Xe \quad . \qquad (1)$$

$$Xe_3 \xrightarrow{D_0(Xe_3)} Xe_2 + Xe \xrightarrow{IP(Xe_2)} Xe_2^+ + Xe$$

To a first approximation, $D_0(Xe_3)$ can be taken as the Xe_2 dissociation energy which is 0.024 eV.[5] The dissociation energy of Xe_3^+ is 0.27(2) eV[7] and the adiabatic IP of Xe_2 is 11.13(1) eV.[8] Hence, the adiabatic IP of Xe_3 is ∿ 10.88(4) eV. From Ref. 1, the Xe_2 electron appearance potential was determined to be 11.76 ± 0.01 eV. The present work shows that the Xe_3 electron appearance potential is 11.30 ± 0.05 eV. Thus, as the cluster size increases from dimer to trimer, the electron appearance potential moves closer to the adiabatic IP. Furthermore, the solid-state Xe photoemission data of Schwentner et al. indicate that the threshold for photoemission[9] and the photoelectron energy distribution curves[10] yield identical appearance potentials, confirming the limit of this trend

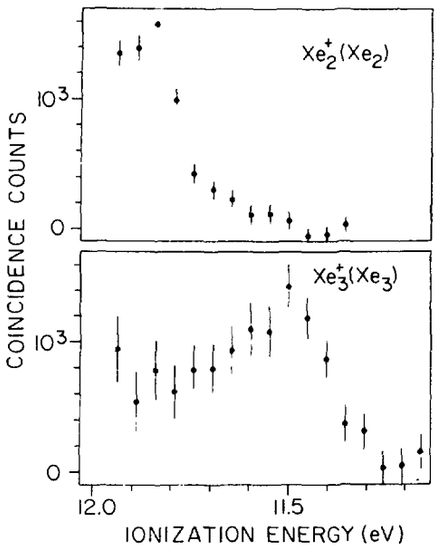

FIG. 1.--Photoelectron-photoion coincidence spectra of Xe_2 and Xe_3. The $Xe^+ {}^2P_{3/2}$ state is at 12.130 eV.

as the "infinite cluster" is approached.

These observed features will serve as demanding tests for theoretical treatments of atomic clusters. (See, for example, Refs. 6, 11, 12.) As the sizes of the clusters studied more thoroughly bridge the gap between free atoms and solids, the trends that exist as condensation proceeds will become more apparent. Furthermore, the coincidence technique will serve as an important complement to related techniques. Studies on surface-supported clusters[13] can be compared with the gas-phase coincidence spectra discussed in this paper to assess substrate-overlayer interactions, which can be significant.[14] In a similar way, matrix-cluster interactions can be assessed which may be present in matrix isolation experiments.[15,16] The interplay of the coincidence technique with other methods undoubtedly will be a critical aspect of future studies.

References

1. P. M. Dehmer and J. L. Dehmer, J. Chem. Phys. 68, 3462 (1978).
2. A. van Deursen and J. Reuss, Int. J. Mass. Spectrom. Ion Phys. 23, 109 (1977).
3. E. D. Poliakoff, P. M. Dehmer, J. L. Dehmer, and R. Stockbauer, to be published.
4. W. R. Wadt, private communication.
5. J. A. Barker, R. O. Watts, J. K. Lee, T. P. Schafer, and Y. T. Lee, J. Chem. Phys. 61, 3081 (1974).

6. W. R. Wadt, Appl. Phys. Lett., in press.
7. H. Helm, Phys. Rev. A 14, 680 (1976).
8. C. Y. Ng, D. J. Trevor, B. H. Mahan, and Y. T. Lee, J. Chem. Phys. 65, 4327 (1976).
9. N. Schwentner, M. Skibowski, and W. Steinmann, Phys. Rev. B 8, 2965 (1973).
10. N. Schwentner, F.-J. Himpsel, V. Saile, M. Skibowski, W. Steinmann, and E. E. Koch, Phys. Rev. Lett. 34, 528 (1975).
11. D. R. Salahub and R. P. Messmer, Phys. Rev. B 16, 2526 (1977).
12. R. L. Martin and E. R. Davidson, Mol. Phys. 35, 1713 (1978).
13. S.-T. Lee, G. Apai, M. G. Mason, R. Benbow, and Z. Hurych, Phys. Rev. B 23, 505 (1981); M. G. Mason, L. J. Gerenser, and S.-T. Lee, Phys. Rev. Lett. 39, 288 (1977) and 39, 1372 (1977); G. Apai, J. F. Hamilton, J. Stohr, and A. Thompson, Phys. Rev. Lett. 43, 165 (1979).
14. C. P. Flynn and Y. C. Chen, Phys. Rev. Lett. 46, 447 (1981).
15. M. Moskovits and D. P. LiLella, J. Chem. Phys. 72, 2267 (1980).
16. G. A. Thompson and D. M. Lindsay, J. Chem. Phys. 74, 959 (1981); D. M. Lindsay, D. R. Herschbach, and A. L. Kwiram, Mol. Phys. 32, 1199 (1976).

POLARIZATION OF FLUORESCENCE FOLLOWING MOLECULAR PHOTOIONIZATION*

E. D. Poliakoff, J. L. Dehmer, Dan Dill,† A. C. Parr,‡ K. H. Jackson,§ and R. N. Zare§

Molecular photoionization is an inherently anisotropic process since degenerate ionization pathways have different symmetries and, in general, different dipole strengths. This anisotropy will manifest itself by partial alignment of the residual ion which depends only upon the relative dipole strengths of the alternative photoelectron channels. We show that this alignment of molecular ions can be probed directly by measuring the polarization of their fluorescence, and that this polarization yields the relative strengths for degenerate photoelectron channels. To demonstrate the effect, we report the first such measurement, for the N_2^+ $B^2\Sigma_u^+$ state produced by photoionization of N_2 in the range 450 Å < λ < 660 Å, and compare the results with model calculations. The excitation-fluorescence sequence studied is given by

$$N_2(X\ ^1\Sigma_g^+) + h\nu \rightarrow N_2^+(B\ ^2\Sigma_u^+) + e^-(\varepsilon\sigma_g, \varepsilon\pi_g) \rightarrow N_2^+(X\ ^2\Sigma_g^+) + h\nu' \quad . \qquad (1)$$

In this case, photoionization proceeds via σ_g (parallel) and π_g (perpendicular) transition dipoles.[1] A quantum-mechanical analysis[2] shows that the fluorescence polarization is given by

$$P = (\sigma_{\parallel} - \sigma_{\perp})/(\sigma_{\parallel} + \sigma_{\perp}) \quad , \qquad (2)$$

where $\sigma_{\parallel}$ and $\sigma_{\perp}$ are the cross sections for production of the B state followed by its decay to the X state by fluorescence polarized parallel and perpendicular to the incident ε-vector, respectively. These cross sections are given by

---

*Summary of an article published in Phys. Rev. Lett. 46, 907 (1981).

†Consultant, Radiological and Environmental Research Division. Permanent address: Department of Chemistry, Boston University, Boston, MA 02215.

‡National Bureau of Standards, Washington, D.C. 20234.

§Department of Chemistry, Stanford University, Stanford, CA 94305.

$$\sigma_q = \sigma(B \to X) \sum_{j_f j_*} (2j_* + 1)^2 (j_* 0, 10 | j_f 0)^2$$

$$\times \sum_{t_\gamma t_i} (2t_i + 1)^{-1} (10, 1q | t_\gamma q)^2 \begin{Bmatrix} 1 & 1 & t_\gamma \\ t_i & j_f & j_* \end{Bmatrix}^2 \times \sum_{\ell\mu\mu'} D^{-*}_{\ell\mu'\mu'} D^{-}_{\ell\mu\mu}$$

$$\times (1\mu', j_* 0 | t_i \mu')(1\mu, j_* 0 | t_i \mu)(\ell\mu', j_i 0 | t_i \mu')(\ell\mu, j_i 0 | t_i \mu) \quad . \tag{3}$$

Here, the $D^{-}_{\ell\mu\mu}$, defined in Eq. 3 of Ref. 3 are photoionization amplitudes for ejection of an electron with asymptotic orbital momentum $\vec{\ell}$ and with projection μ along the molecular axis of both $\vec{\ell}$ and the dipole interaction. The quantum numbers, j_i, j_*, and j_f, give the rotational momenta of the initial neutral N_2, the excited N_2^+, and the final (ground-state) N_2^+. The angular correlation between the ionization and fluorescence dipole interaction can hava harmonics $t_\gamma = 0,1,2$. The angular momentum transferred from the ionizing dipole interaction to the excited state molecular rotation is $\vec{t}_i$. The polarization is parallel for $q = 0$ and perpendicular for $q = \pm 1$. Finally, the fluorescence cross section is represented by $\sigma(B \to X)$. The result is for the $\Sigma \to \Sigma \to \Sigma$ transition sequence studied here. The general expression and its fuller discussion will be presented in a subsequent publication.[2]

For completeness, we note that a classical formulation also predicts a polarization in fluorescence.[4] If D^2_σ and D^2_π are the dipole strengths for σ and π continuum channel ionizations, respectively, and we define $R \equiv D^2_\pi / D^2_\sigma$, then

$$P^{\text{classical}} = (1 - R)/(7 + 13R) \quad . \tag{4}$$

To illustrate the general behavior of the new theoretical formulation presented in Eq. 3, we will use dipole amplitudes $D^{-}_{\ell\mu\mu}$ calculated using the multiple scattering model (MSM).[3] We emphasize, however, that Eq. 3 represents a general theoretical framework which can be evaluated using dipole strengths computed from a whole hierarchy of approximations, from the model calculation used here to much more sophisticated calculations incorporating electron correlation, vibrational effects, etc. We see from Eq. 3 that, in the quantum

mechanical formulation, the polarization depends both on the dipole strengths $D_\sigma^2 \equiv \sum_\ell |D^-_{\ell 00}|^2$ and $D_\pi^2 \equiv \sum_\ell |D^-_{\ell \pm 1 \pm 1}|^2$, and on the interference of the dipole amplitudes for a given ℓ. However, numerical evaluation of Eq. 3 shows that for $j_i \geq 5$ the interference terms have negligible effect, i.e., except for very low temperatures, the polarization depends only on the dipole strength ration D_π^2/D_σ^2 (Figure 1a). Furthermore, for $j_i \geq 5$, the polarization computed from Eq. 3 agrees precisely with that derived from the classical formulation, Eq. 4 (see dashed curve in Figure 1b). The $j_i = 3$ and 4 curves are not shown in Figure 1b, but lie just above the $j_i = 5$ curve. Note that a Boltzmann-weighted average is not shown in Figure 1b but is accurately represented by the $j_i = 5$ curve. For low j_i, the quantal rotational motion and the interference terms combine to yield polarizations greater than the classical prediction, especially for $j_i = 0$ for which $P \sim 20\%$ over a very large energy range. This predicted temperature dependence could be experimentally tested by using a supersonically-cooled expansion. We are planning such an arrangement for future studies.

The experimental apparatus has been described previously.[3] The experimental results are shown in Figure 1b. Referring to Fig. 1b, the threshold for the $B\ ^2\Sigma_u^+$ state production is at 18.757 eV;[5] data were also taken between 4 and 8 eV kinetic energy, but this region contains many autoionizing resonances[6] which could distort the results. However, data taken on a 0.25 energy mesh near the 554.1 Å resonance revealed no discernible resonance structure in the polarization dependence. We see that the observed polarization is positive and decreases with increasing photon energy; the highest degree of polarization measured was $P = 0.052 \pm 0.003$ at an energy of 0.7 eV above threshold. Clearly all of the experimental points in Figure 1b lie substantially below the predictions ($j_i = 5$) based on the MSM model. This, in turn, implies the experimentally deduced D_π^2/D_σ^2 ratios will be larger than the theoretical ones, as indicated in Figure 1a. On the one hand, the agreement between the MSM-level calculation and experiment is poor, and clearly indicates the need for improved calculations of the dipole amplitudes. On the other hand, the MSM calculation serves to exhibit basic aspects of the theory in Eq. 3 and acts as a point of reference for future improvements as follows. First, the model calculation properly reflects

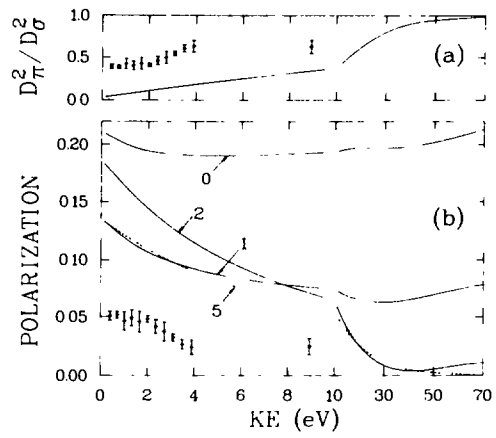

FIG. 1.--Energy dependence of D_π^2/D_σ^2 and the polarization, P, for the $N_2^+(B\ ^2\Sigma_u^+)$ state. The photon energy corresponding to the zero of the graph is 18.757 eV (see Ref. 5). Note that the energy scale changes at 10 eV kinetic energy. (a) MSM predictions and experimental determination for D_π^2/D_σ^2; (b) MSM predictions and experimental determinations for P. The numbers refer to the value of j_i. The $j_i = 5$ curve is dashed and is indistinguishable from the classical result using the MSM dipole strengths.

the positive slope of D_π^2/D_σ^2 at low energies and the approach of this ratio to unity at high energy, where the dynamics are dominated by the spherical environment in the atomic cores. The general increase in D_π^2/D_σ^2 at low energy is caused by the suppression near threshold of the d-wave lead term of the π_g continuum wave function by centrifugal forces. Second, future improvement in the calculation can be confined to computing better dipole amplitudes, which can then be transformed into the observable polarization by use of Eq. 3. The inaccuracy in the MSM-based amplitudes are, of course, a consequence of the approximations implicit in the MSM model;[3] however, we note that $2\sigma_u$ photoionization in N_2 appears to be a somewhat pathological case, e.g., the photoelectron symmetry parameters for this channel were by far the worst in an MSM treatment[3] of the valence levels of N_2. This might imply the problem traces to electron correlation effects or nuclear motion effects. Two possibilities are <u>inter</u>channel coupling with states[7] associated with the $C\ ^2\Sigma_u^+$ state of N_2^+ and <u>intra</u>channel coupling which would redistribute the π_g oscillator strength distribution whose concentration in the $1\pi_g$ valence state by the centrifugal barrier[3] is probably overemphasized by a one-electron treatment. Third, as the temperature-dependent effects derive mainly from geometric considerations, implicit in Eq. 3, the qualitative aspects of the temperature dependence in Figure 1b are valid, although the quantitative aspects are suspect, owing to the inaccurate D_π^2/D_σ^2 ratio used here.

In conclusion, the measurement of fluorescence polarization following molecular photoionization to excited states yields the <u>ratio</u> of dipole strengths

for degenerate ionization channels. This experiment is the newest member of a class of experiments which probes the alignment of atomic[8,9] and molecular[10] ions and which, by virtue of not detecting (integrating over) the photoelectron ejection angle, are independent of the relative phases of the ionization channels. Though these techniques have yet to be extensively exploited, they are important complements to the traditional measurements of photoelectron branching ratios and angular distributions, providing the additional information necessary to determine the magnitudes and phases of dipole transition amplitudes separately. Combining these complementary probes will therefore lead to a new level of understanding of molecular photoionization dynamics.

We wish to thank Dr. M. G. White and Dr. S. Wallace for helpful discussions and S. Wallace for valuable assistance in evaluating Eq. 3. We are grateful to Dr. R. P. Madden and the staff of the NBS-SURF II facility for their generous cooperation during this work.

References

1. G. Herzberg, Spectra of Diatomic Molecules, Van Nostrand Reinhold Co., New York (1950).
2. D. Dill, to be published.
3. D. Dill and J. L. Dehmer, J. Chem. Phys. 61, 692 (1974). J. L. Dehmer and D. Dill, Electron-Molecule and Photon-Molecule Collisions, T. Rescigno, V. McKoy, and B. Schneider, Eds., Plenum Publ. Corp., New York (1979); S. Wallace, D. Dill, and J. L. Dehmer, J. Phys. B 12, L417 (1979); J. L. Dehmer, D. Dill, and S. Wallace, Phys. Rev. Lett. 43, 1005 (1979).
4. E. D. Poliakoff, J. L. Dehmer, D. Dill, A. C. Parr, K. H. Jackson, and R. N. Zare, Phys. Rev. Lett. 46, 907 (1981).
5. G. R. Cook and P. H. Metzger, J. Chem. Phys. 41, 321 (1964).
6. K. Codling, Astrophys. J. 143, 552 (1966).
7. A. L. Roche and J. Tellinghuisen, Mol. Phys. 38, 129 (1979) and references therein.
8. C. D. Caldwell and R. N. Zare, Phys. Rev. A 16, 255 (1977); H. Klar, J. Phys. B 13, 2037 (1980); W. Mauser and W. Mehlhorn, to be published.
9. S. Flugge, W. Mehlhorn, and V. Schmidt, Phys. Rev. Lett. 29, 7 (1972).
10. J. L. Dehmer and D. Dill, Phys. Rev. A 18, 164 (1978).

ABSORPTION CROSS SECTIONS OF THE CHLOROMETHANES FROM THRESHOLD TO 21 eV*

J. C. Person, P. P. Nicole, and D. E. Fowler†

The chloromethanes are an important class of industrial chemicals, and they are sources of chlorine atoms for atmospheric photochemistry. We report our measurements of the absorption cross section σ for methyl chloride, methylene chloride (CH_2Cl_2), chloroform ($CHCl_3$), and carbon tetrachloride from the absorption threshold (near 6 eV) up to 21 eV.

Two experimental techniques were used. For photon energies below 11.7 eV, the measurements were made in an 8.49-cm long absorption cell with LiF windows; the split-beam detector system[1] uses sodium salicylate fluorescence and two photomultipliers to measure the light absorption. At energies above the ionization potential, we used a windowless dual ion chamber with the front chamber 7.39 cm long and the rear chamber 21.07 cm. The monochromator was a McPherson Model 225, and the bandpass was 0.09-nm FWHM. The light sources were a hydrogen discharge, used for energies below 13.2 eV, and a helium continuum for energies above 12.6 eV. Capacitive manometers (Baratrons) from MKS Instruments were used to measure the gas pressures, and the 1-torr Baratron was calibrated with an oil manometer.

An overall view of the data is given by Figure 1, which shows a plot of σ, where 1 Mb = 10^{-18} cm^2, over the entire energy range. For regions with sharp structure, it is uncertain whether the bandpass is narrow enough to avoid line-saturation errors. The data shown in Figure 1 for each gas consists of a composite of results obtained for part of the energy range for four pressures, and have not been averaged over multiple runs. Furthermore, the data from the windowed cell are not in final form in respect to energy-scale adjustments, or for corrections for light that is reflected at the windows and for gas fluorescence;

---

*Summary of a paper presented at the VI International Conference on Vacuum Ultraviolet Radiation Physics, Charlottesville, Virginia June 2-6, 1980.

†Undergraduate Research Participant from Macalester College, St. Paul. MN 55101.

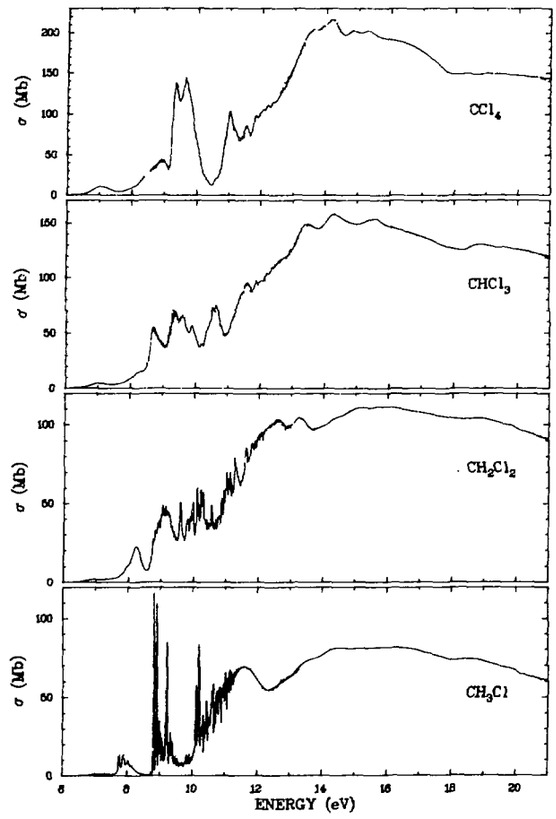

FIG. 1.--Absorption cross sections of CCl_4, $CHCl_3$, CH_2Cl_2, and CH_3Cl as functions of photon energy.

in addition, the pressure gauge has not been recalibrated recently. Presumably, these corrections and/or better corrections for scattered light will explain our observation that the ion-chamber data are 4 to 7% higher in the energy region where both techniques were used.

The linear scale of the figure makes it difficult to see the first few absorption bands, but it does show the strength of the absorptions in the higher energy region. The sharp absorption features become less numerous with increasing chlorine substitution. These features are mainly Rydberg-series members;[2-7] many of the broad peaks and shoulders at higher energies can be assigned to transitions to the low-lying members of Rydberg series that converge on the higher ionization potentials.[8]

References

1. R. W. Ditchburn, J. Quant. Spectrosc. Radiat. Transfer 2, 361 (1962).

2. W. C. Price, J. Chem. Phys. 4, 539 (1936).
3. C. R. Zobel and A.B.F. Duncan, J. Am. Chem. Soc. 77, 2611 (1955).
4. B. R. Russell, L. O. Edwards, and J. W. Raymonda, J. Am. Chem. Soc. 95, 2129 (1973).
5. J. W. Raymonda, L. O. Edwards, and B. R. Russell, J. Am. Chem. Soc. 96, 1700 (1974).
6. P. Hochmann, P. H. Templet, H.-t. Wang, and S. P. McGlynn, J. Chem. Phys. 62, 2588 (1975).
7. S. Felps, P. Hochmann, P. Brint, and S. P. McGlynn, J. Mol. Spectrosc. 59, 355 (1976).
8. A. W. Potts, H. J. Lemka, D. G. Streets, and W. C. Price, Philos. Trans. R. Soc. London 268A, 59 (1970).

MICROCOMPUTER CONTROL OF ABSORPTION EXPERIMENTS*

J. C. Person and P. P. Nicole

An inexpensive microcomputer system is used to control experiments that measure photoabsorption cross sections. The control includes positioning the monochromator wavelength, positioning a filter wheel, controlling valves to change the gas sample, timing the photomultiplier counters, and reading data giving the temperature, pressure, and counter readings. The data are written on magnetic tape after correction for effects such as counter dead time, scattered light, and dark counts. Analog signals are output to a chart recorder to give a visual presentation of the absorption spectrum and the lamp intensity.

There are several choices available for small computers to control laboratory experiments. We believe that one of the major advantages of having a small computer is the flexibility possible if one can rapidly change the computer programming. This flexibility is especially valuable during the setup of a new experiment when the operating procedures are being tested; flexibility is even more important when the computer has enough capacity to do the entire calculation so that the results are immediately available — without waiting for a larger computer to process the data. Thus, we recommend choosing a computer system sophisticated enough to have convenient software, yet simple enough to be independent of outside help. The computer system should also be modular to permit easy additions.

We believe that a computer system using the S-100 bus and the 8080 or Z-80 microcomputer chip represents a good choice because of the wide variety of low-cost components and software available. We recommend starting with an 8" floppy-disk drive (two drives are a very good investment for ease in making back-up disks and for certain other operations during software development). An essential companion of the disk drive(s) is the disk-operating system, such

*Summary of a paper presented at the VI International Conference on Vacuum Ultraviolet Radiation Physics, Charlottesville, Virginia, June 2-6, 1980.

as the CP/M or MP/M software from Digital Research.* We also recommend a FORTRAN compiler, as BASIC interpreters are often too slow and assembly-language programs are time-consuming to develop.

There are plug-in cards available for the S-100 bus fur tasks such as analog-to-digital conversion (ADC), digital-to-analog conversion (DAC), parallel and serial input/output (I/O) ports, and real-time clocks. Voltages from pressure-measuring instruments, etc., can be input to a multiplexed ADC to provide data to the computer, and parallel I/O ports can usually be connected to any device that provides digital outputs.

We have found that the printing counters manufactured by EG&G Ortec, Inc.† can be easily interfaced to two parallel I/O ports, and the Ortec Model 779 interface/controller module is not required in our application. With an 8080 microcmoputer with a 2-MHz clock rate, the rate of transfer of data is more than 16,000 digits/s, which is greater than the 1920-digits/s maximum rate of the Ortec Model 779. We should also point out that this interface does not require the printing counter to have the parallel-output option.

During the initial setup of the computer system, it is desirable to have expert help, as there may be machine and programming errors, and it is very difficult to learn a new system when it is not working properly. However, once the system is set up, the user can soon become nearly independent of outside experts. We have used static, rather than dynamic, memory, and we have found no problems of compatibility when using components supplied by different manufacturers. Furthermore, we have found the system to be quite reliable — aside from a few failures during the breaking-in period.

In one test case, we found a FORTRAN program about ten times slower in our 8080 than on a PDP 11/60 and about 100 times slower than on an IBM 3033A under CMS. A BASIC version of the same program ran in our machine about 50 times slower. However, with the FORTRAN program, we are able to read in data from two counters and a digital thermometer, as well as voltages giving the

---

*Digital Research, Box 579, Pacific Grove, CA 93950.

†EG&G Ortec, Inc., 100 Midland Road, Oak Ridge, TN 37830.

pressure measured by two sensors. The program subtracts the dark counts, corrects for the dead times, calculates the gas density as well as the absorption cross section, and sends pulses to the wavelength-stepping motor — all in a time of 2 to 3 s. We usually count for 10 s or more at each point, and, if we operate the counter-timer using interrupts, we have nearly all of the counting time available for calculations so that we could make even more sophisticated data corrections.

We position the monochromator wavelength by using a parallel output port to send impulses to the up or down inputs (photo-isolated) on a stepping motor translator module. The filter wheel is mounted on one lid of the McPherson Model 225 monochromator, and it is dirven by a rotary solenoid through a rotary vacuum feedthrough and a right-angle drive. The 115-V power on the solenoid coil is controlled by a photo-isolated, solid-state relay* with zero-voltage AC turn-on, and the relay is controlled by a parallel output port. We also use these relays to control the solenoid valves on our gas-handling system. Thus, with an S-100 main frame, an 8080 or Z-80 CPU, 32 to 64 k of memory, a dual floppy-disk system, some I/O ports -- along with the ADC and DAC, and some software, one can assemble a rather powerful computing facility for $5000 to $7000 or $6000 to $9000 if one includes a terminal.

Reference

1. J. C. Person and P. P. Nicole, Rev. Sci. Instrum. 51, 1425 (1980); also this report.

*Opto 22, 5842 Research Drive, Huntington Beach, CA 92649

INTERFACE FOR RAPID DATA TRANSFER FROM NIM COUNTERS TO SMALL COMPUTERS

James C. Person and Paul P. Nicole

The printing counters manufactured by EG&G Ortec, Inc.[†] (and similar companies such as Tennelec, Inc.[‡]) feature data outputs that can be connected in a print loop with up to 50 different modules daisy-chained together. These loops usually connect to a serial interface controller, such as the Ortec Model 779 interface-controller module or the Tennelec Model TC 588 buffered printer interface module, and the small computer then communicates with the controller via a serial input-output (I/O) port. The serial link may be required if the data must be transmitted over a large distance, but this limits the rate of data transfer to 1920 digits/s. We have found that it is not necessary to use an interface-controller module, and we wire the print loop data and control lines directly to two parallel I/O ports on our small computer. One of the features of the Ortec and Tennelec printing counters is that all of the data are transferred one digit at a time over four data lines, which is more convenient than when the data must be transferred with four separate lines for each digit. The print loop also has three control lines for the data transfer, and there are two more controls for the gate and reset lines on the counters. As a result, the interconnecting wiring involves only four data lines to a parallel input port and five control lines to a parallel output port.

The specific interface we constructed is for use with two Ortec Model 770 counters which are 6-decade scalers in standard NIM modules. These counters should be representative of any of the modules that are compatible with the Ortec print loop. Our small computer uses the Intel 8080 COU chip, and we have tried two different types of parallel I/O ports: one uses the Motorola MC6820 IC (integrated circuit) and one uses the Intel 8212 IC. If pull-up resistors are not already installed on the port, then they must be installed for

---

[†]EG&G Ortec, Inc., 100 Midland Road, Oak Ridge, TN 37830.

[‡]Tennelec, Inc., 601 Turnpike, Oak Ridge, TN 37830.

the four data lines in the print loop, since the Model 770 counter uses Signetics 8881 gates, which have bare output collectors. The resistance value[1] should be in the range of 300 to 1600 ohms; larger resistors can be used if the number of modules in the print loop is less than 50. In addition, we found that installation of a 1-kohm resistor controlled the noise problems we experienced on the print-advance lines.

The programming of the 8080 IC consists of a subroutine to initialize the I/O ports, if necessary, and a series of subroutines to start, stop, and reset the counters, and a subroutine to control the print, print advance, and previous-module-finished lines so as to read in the four bits of binary-coded-decimal (BCD) data for each digit in the print loop. This routine also does a logical .OR. between the data and 30_{16}, which converts the BCD representation into the ASCII representation of the digit. The ASCII digits are then stored in memory in an array that is ready for printing or to be read by FORTRAN programs for data manipulations. This subroutine transfers and converts the 12 digits from our two counters in 0.68 mn, or more than 17k digits/s.

In conclusion, this interface is easy to install, it permits rapid data transfer, and it saves the cost of a separate interface-controller module.

Reference

1. DCL Series 8000 Handbook, Signetics Corporation, Sunnyvale, CA, Sec. 4-5 (May 1968).

MEASUREMENT OF β VALUES AND BRANCHING RATIOS IN THE REGION OF THE $3s3p^64p\ {}^1P^o_1$ RESONANCE IN Ar AND THE $5s5p^66p\ {}^1P^o_1$ RESONANCE IN Xe*

K. Codling,† J. B. West,‡ A. C. Parr,§ J. L. Dehmer, and R. L. Stockbauer§

Variations in asymmetry parameter, β, and the ratio of partial photoionization cross sections $\sigma(^2P_{3/2}):\sigma(^2P_{1/2})$ have been determined in the region of the

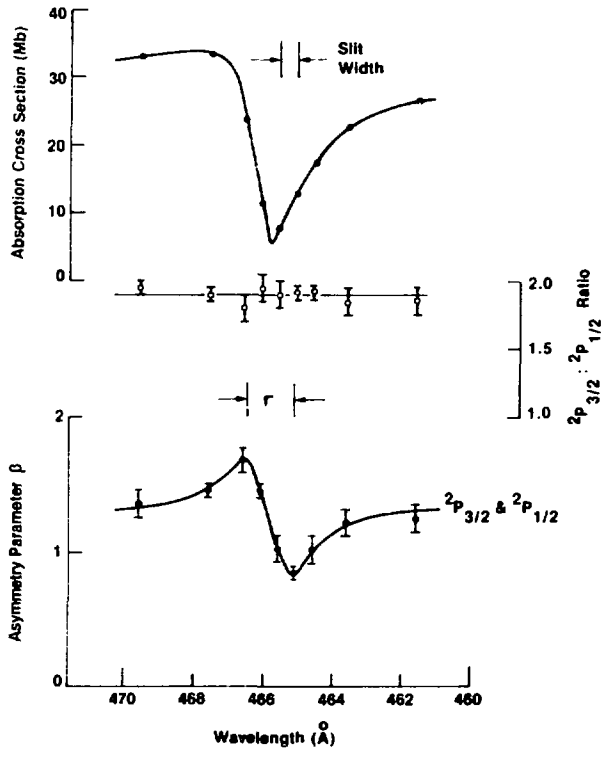

FIG. 1.--The photoabsorption (photoionization) cross section (top), branching ratio $\sigma(^2P_{3/2}):\sigma(^2P_{1/2})$ (middle) and asymmetry parameter β (bottom) for the 3p electrons in Ar in the region of the $3s3p^64p\ {}^1P^o_1$ resonance.

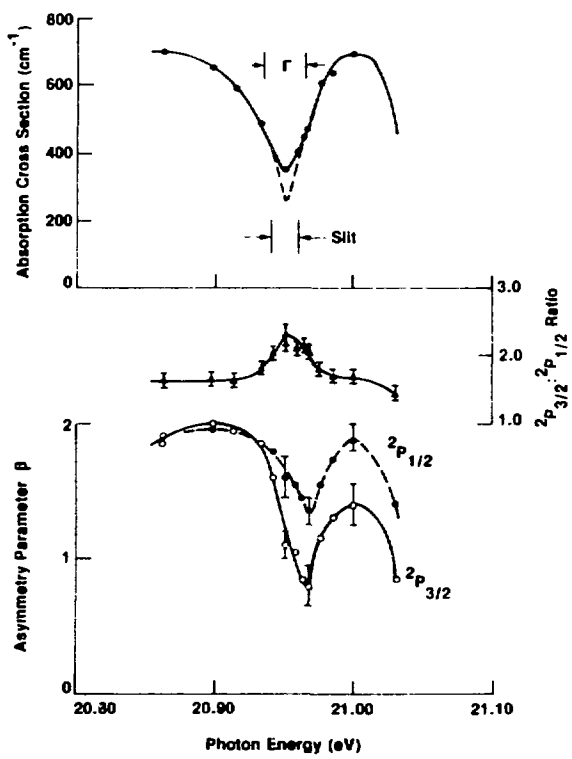

FIG. 2.--The photoabsorption (photoionization) cross section (top), branching ratio $\sigma(^2P_{3/2}):\sigma(^2P_{1/2})$ (middle) and asymmetry parameter β (bottom) for the 5p electrons in Xe in the region of the $5s5p^66p\ {}^1P^o_1$ resonance.

---

*Summary of a paper published in J. Phys. B 13, L693 (1980).

†Physics Department, University of Reading, Whiteknights, Reading, RG6 2AF, England.

‡Daresbury Laboratory, Science Research Council, Daresbury, Warrington, WA4 4AD, England.

§National Bureau of Standards, Washington, D.C. 20234.

$3s3p^6 4p\ {}^1P_1^o$ resonance in Ar (Figure 1) and the $5s5p^6 6p\ {}^1P_1^o$ resonance in Xe (Figure 2). In both cases there is a considerable variation in β through the resonance. In Ar the β values for the spin-orbit components are similar, in Xe significantly different. In Xe, the branching ratio shows a modest variation through the resonance, whereas in Ar no noticeable change occurs.

TRIPLY-DIFFERENTIAL PHOTOELECTRON STUDIES OF MOLECULAR AUTOIONIZATION PROFILES. THE 710 Å - 730 Å REGION OF THE N_2 SPECTRUM *

A. C. Parr,† D. L. Ederer,† B. E. Cole,‡ J. B. West,§ R. Stockbauer,† K. Codling,‖ and J. L. Dehmer

---

We report photoelectron studies of molecular autoionization resolved into position within the resonance profile, photoelectron ejection angle, and final vibrational state. Using the first members of prominent window and absorption series converging to $N_2^+ B\ ^2\Sigma_u^+$ as an example, we demonstrate striking variations of vibrational branching ratios and photoelectron asymmetry parameters within autoionizing profiles. Such triply-differential data represent a very detailed characterization of the rovibronic interactions governing molecular autoionization.

In Figure 1 we present the vibrational branching ratios for formation of the ground state ion $N_2^+ X\ ^2\Sigma_g^+$ by photoionization in the 710 Å ≤ λ ≤ 730 Å range.

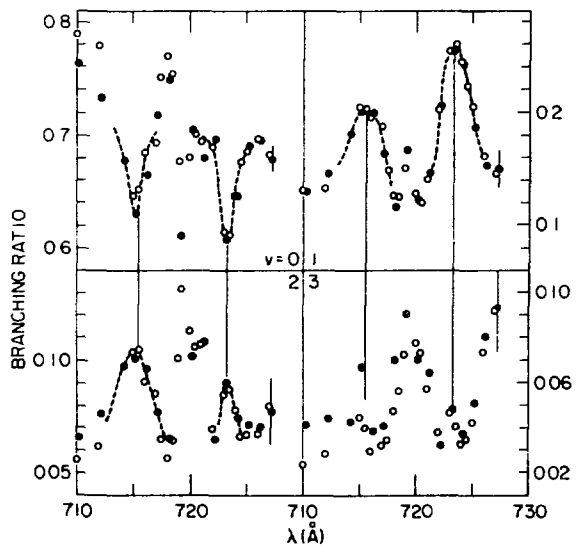

FIG. 1.--Vibrational branching ratios for production of $N_2^+ X\ ^2\Sigma_g^+$ (v_o = 0-3) in the range 710 Å ≤ λ ≤ 730 Å. Vertical lines at 715.5 Å and 723.3 Å denote the positions of the first members of the Hopfield "emission" and absorption series approaching the $N_2^+ B\ ^2\Sigma_u^+$ (v = 0) limit. Typical error bars are indicated on the last point in each frame. The dashed line is hand-drawn to guide the reader's eye. Open and closed circles represent two independent runs.

---

*Summary of a letter published in Phys. Rev. Lett. 46, 22 (1981) and a paper published in J. Phys. B 14, 1791 (1981).

†National Bureau of Standards, Washington, D.C. 20234.

‡Honeywell Corporate Technology Center, Bloomington, Minn. 55420.

§Daresbury Laboratory, Science Research Council, Daresbury, Warrington, WA4 4AD, England.

‖J. J. Thomson Physical Laboratory, University of Reading, Reading RG6 2AF, England.

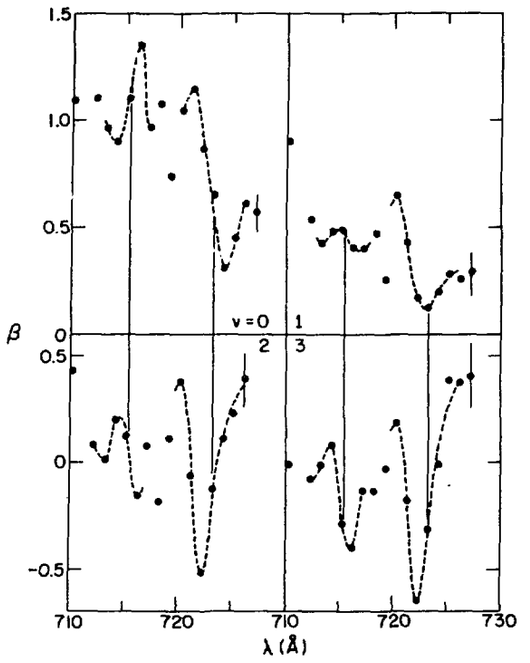

FIG. 2.--Photoelectron asymmetry parameters corresponding to producing $N_2^+ X\ ^2\Sigma_g^+$ (v = 0-1) in the range 710 Å $\leq \lambda \leq$ 730 Å. Other conventions as in Figure 1.

Here we define the vibrational branching ratio as the ratio of the intensity of a particular vibrational level to the sum over the whole vibrational band. In Figure 2 the asymmetry parameter β is given for the same process. In both figures the positions of the Hopfield emission and absorption features at 715.5 Å and 723.3 Å, respectively, are indicated by solid lines joining the upper and lower frames. In the vicinity of these features a hand-drawn dashed durve is constructed only to guide the eye, and should not be taken too seriously. In both figures, typical error bars for the data in each frame are shown on the last point. Duplicate branching ratio measurements (the open circles were taken at the magic angle and the solid dots were deduced from the angular distribution measurements) show the reproducibility of the data.

THE EFFECTS OF AUTOIONIZATION ON VIBRATIONAL BRANCHING RATIOS AND PHOTOELECTRON ANGULAR DISTRIBUTIONS IN MOLECULAR PHOTOIONIZATION: THE FORMATION OF THE GROUND STATE OF O_2^+ BETWEEN 574 Å and 600 Å *

K. Codling,† A. C. Parr,‡ D. L. Ederer,‡ R. Stockbauer,‡ J. B. West,§ B. E. Cole,|| and J. L. Dehmer

---

The partial cross sections (branching ratios) for leaving the O_2^+ ion in the ground $X\ ^2\Pi_g$ state have been determined in the region of the v = 0 and v = 1 components of the neutral excited Rydberg state $(2\sigma_u)^{-1}\ 3s\sigma$ at 594.3 and 589.0 Å by photoelectron spectroscopy. These cross sections have been further subdivided into partial cross sections for leaving the ion in a particular vibrational state. Moreover, the asymmetry parameter, β, has been determined for each vibrational component in this limited spectral range. Considerable variations in both cross section and β are observed. As an example, the variation in β with vibrational quantum number is illustrated in Figure 1 at 593 Å.

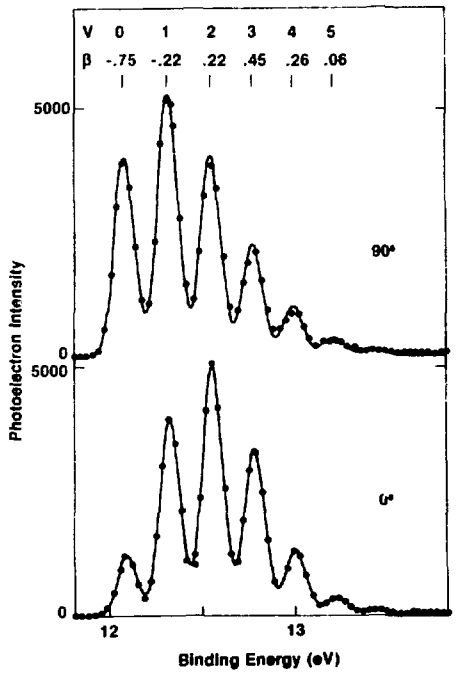

FIG. 1.--The photoelectron spectrum of the O_2^+ $X\ ^2\Pi_g$ state at an incident photon energy of 593 Å for two angles, θ = 0° and θ = 90°. The β value for each vibrational level is given at the top of the figure.

---

* Summary of an article published in J. Phys. B 14, 657 (1981).

† J. J. Thomson Physical Laboratory, University of Reading, Reading RG6 2AF England.

‡ National Bureau of Standards, Washington, D.C. 20234.

§ Science Research Council, Daresbury Laboratory, Warrington WA4 4AD, England.

|| Honeywell Corporate Technology Center, Bloomington, Minn. 55420.

VIBRATIONAL-STATE DEPENDENCE OF PARTIAL CROSS SECTIONS AND PHOTOELECTRON ANGULAR DISTRIBUTIONS THROUGH AUTOIONIZING RESONANCES: THE n=3 RYDBERG STATE OF THE B $^2\Sigma^+$ STATE OF CO^+ *

D. L. Ederer,† A. C. Parr,† B. E. Cole,‡ R. Stockbauer,† J. L. Dehmer, J. B. West,§ and K. Codling||

The branching ratios for leaving the CO^+ ion in a particular vibrational level of the ground X $^2\Sigma^+$ state have been determined as a function of photon energy through the n = 3 Rydberg state of the B $^2\Sigma^+$ state of CO^+ (722 Å < λ < 729 Å). These branching ratios have been converted into absolute partial cross sections by normlaizing to existing data obtained using line sources. The asymmetry parameter β has also been determined for each vibrational level in this spectral range. Considerable variations in both have been observed in the region of this resonance.

---

*Abstract of a paper to be published in Proc. R. Soc. (London).

†National Bureau of Standards, Washington, D.C. 20234.

‡Honeywell Corporate Technology Center, Bloomington, Minn. 55420.

§Daresbury Laboratory, Science Research Council, Daresbury, Warrington, WA4 4AD, England.

||J. J. Thomson Physical Laboratory, University of Reading, Reading, RG6 2AF, England.

SHAPE RESONANCES IN MOLECULAR FIELDS*

J. L. Dehmer and Dan Dill†

Shape resonances are quasibound states in which a particle is temporarily trapped by a potential barrier, through which it may eventually tunnel and escape. In molecular fields, such states can result from so-called "centrifugal barriers," which block the motion of otherwise free electrons in certain directions, trapping them in a region of space with molecular dimensions. In recent years, there has been a flurry of studies of shape resonance effects in both molecular photoionization and electron-molecule scattering. The important role of shape resonances in these processes stems from several key factors: First, they are being identified in the spectra of a growing and diverse collection of molecules and now appear to be present somewhere in the spectra of most molecules. Second, owing to their localized quasibound nature, such resonances often produce intense, easily studied features. Third, resonant trapping usually imparts a well-defined orbital momentum character to the escaping electron which may be reflected in characteristic angular distributions. Last, but not least, the essentially one-electron nature of the phenomenon lends itself to theoretical treatment by realistic, independent-electron methods, with the concomitant flexibility in terms of complexity of molecular systems, energy ranges, and alternative physical processes.

Within the last year or so, studies of the interplay between shape resonances and molecular vibration have led to the prediction[1-3] and experimental confirmation[4-8] of new shape resonance effects in both molecular photoionization and electron-molecule scattering. At the most basic level, these effects arise because

---

*Summary of invited talks presented at (a) 11th Annual DEAP Meeting, 10-12 December 1979, Houston, Texas; (b) March APS Meeting, 24-28 March 1980, New York, N.Y.; (c) Molecular Spectroscopy and Dynamics with Synchrotron Radiation—A European Workshop, 29 September-1 October 1980, Maria Laach, West Germany; and (d) 33rd Annual Gaseous Electronics Conference, 7-10 October 1980, Norman, Oklahoma.

†Consultant, Radiological and Environmental Research Division. Permanent address: Department of Chemistry, Boston University, Boston, MA 02215.

the quasibound shape resonance exhibits dramatic changes in position and profile as the internuclear separation varies over the range of the ground state vibration. This causes a breakdown of the Franck-Condon separation of electronic and nuclear motion with the following effects:

In molecular photoionization, it was predicted[1] that vibrational intensities would exhibit large deviations from their Franck-Condon factors (formerly considered a fairly accurate guide in the absence of autoionization effects), over a spectral range which could be several times larger than the resonance halfwidth. Moreover, it was predicted that photoelectron angular distributions for different final vibrational states would differ in a systematic way.[1] These basic predictions were immediately confirmed experimentally[4,6-8] and have a far-reaching impact on our understanding of the dynamics of molecular photoionization.

In electron-molecule scattering, it has been known for some time that shape resonances are very effective in inducing vibrational excitation (see, e.g., Ref. 9 and references therein). The new element in this context is the prediction[2] of enhanced vibrational excitation arising from very weak shape resonances at intermediate (10-40 eV) incident energy. Shape resonances in this energy range lie near the top of their potential barriers and are therefore usually too broad and weak to observe in the vibrationally elastic or total scattering cross section. The key to their discovery was the prediction[2] that they would be prominent in vibrational excitation spectra, to which direct, non-resonant scattering has minimal contribution. This picture is now supported by measurements[5] on the $e\text{-}CO_2$ scattering and earlier $e\text{-}N_2$ results,[10,11] which now take on new meaning.

Expansion, refinement, and unification of these new manifestations of molecular shape resonances have begun in several experimental and theoretical groups, and will provide a stimulating theme in molecular physics in the coming years.

References

1. J. L. Dehmer, Dan Dill, and S. Wallace, Phys. Rev. Lett. 43, 1005 (1979).
2. Dan Dill, J. Welch, J. L. Dehmer, and J. Siegel, Phys. Rev. Lett. 43, 1236 (1979).

3. J. L. Dehmer and Dan Dill, Electronic and Atomic Collisions, Invited Papers from the XIth Int. Conf. on the Physics of Electronic and Atomic Collisions, Kyoto, Japan, 29 August-4 September 1979, N. Oda and K. Takayanagi, Eds., North-Holland Publ., Amsterdam, p. 195 (1980).
4. R. Stockbauer, B. E. Cole, D. L. Ederer, J. B. West, A. C. Parr, and J. L. Dehmer, Phys. Rev. Lett. 43, 757 (1979).
5. M. Tronc, R. Azria, and R. Paineau, J. Physique Lettres 40, L323 (1979).
6. J. B. West, A. C. Parr, B. E. Cole, D. L. Ederer, R. Stockbauer, and J. L. Dehmer, J. Phys. B 13, L105 (1980).
7. B. E. Cole, D. L. Ederer, R. Stockbauer, K. Codling, A. C. Parr, J. B. West, E. D. Poliakoff, and J. L. Dehmer, J. Chem. Phys. 72, 6308 (1980).
8. T. A. Carlson, M. O. Krause, T. Mehaffy, J. W. Taylor, F. A. Grimm, and J. D. Allen, J. Chem. Phys. 73, 6056 (1980).
9. G. J. Schulz, Principles of Laser Plasmas, G. Bekefi, Ed., Wiley, New York, p. 33 (1976).
10. J. L. Dehmer, J. Siegel, J. Welch, and Dan Dill, Phys. Rev. A 21, 101 (1980).
11. Z. Pavlovic, M.J.W. Boness, A. Herzenberg, and G. J. Schulz, Phys. Rev. A 6, 676 (1972).

PICTURES OF UNBOUND MOLECULAR ELECTRONS, INCLUDING SHAPE-RESONANT STATES. EIGENCHANNEL CONTOUR MAPS*

D. Loomba,[†] Scott Wallace,[‡] Dan Dill,[†§] and J. L. Dehmer

Eigenchannel wave functions are identified as the continuum analog of discrete-state eigenfunctions familiar from molecular structure calculations. As examples, eigenchannel wave functions are plotted for shape-resonant and non-resonant eigenchannels of N_2. Both types of functions show charcteristic nodal patterns. The penetration over a narrow energy range of the resonant wave function through a potential barrier into the molecular interior, the key feature of shape-resonant states, is clearly shown for the example of the N_2 f-wave-dominated σ_u shape resonance at 1.2 Ry electron kinetic energy. To illustrate

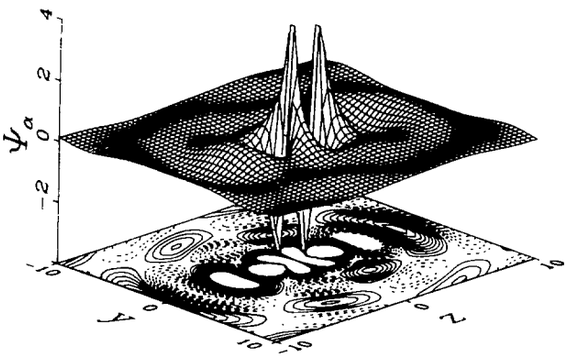

FIG. 1.--N_2 continuum f-wave (ℓ=3) eigenchannel wave function at the resonance energy of 1.2 Ry. The molecule is in the yz plane, along the z axis, centered at y=z=0. Contours mark steps of 0.03 from 0.02 to 0.29; positive = solid, negative = dashed.

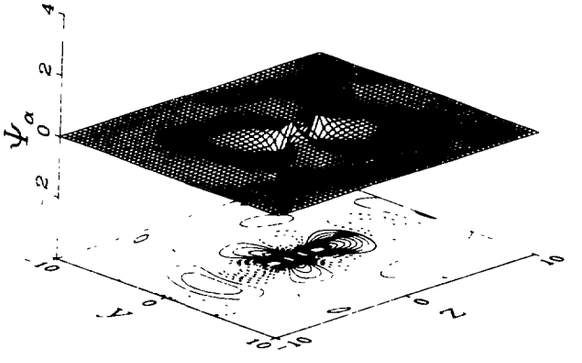

FIG. 2.--Same plot as in Figure 1, only at the off-resonance energy of 0.9 Ry.

*Summary of an article accepted for publication in J. Chem. Phys.

[†]Department of Chemistry, Boston University, Boston, MA 02215.

[‡]Department of Materials Science and Engineering, Massachusetts Institute of Technology, Cambridge, MA 02139.

[§]Consultant, Radiological and Environmental Research Division.

the appearance of a resonant continuum wave function, the eigenchannel contour map for the σ_u channel at the resonance energy is shown in Figure 1. The analogous plot at a non-resonant energy is shown in Figure 2 for contrast. This visualization of continuum electronic amplitudes should prove to be a significant new tool in the study of continuum electron-molecule dynamics.

SHAPE-RESONANT FEATURES IN THE PHOTOIONIZATION SPECTRA OF NO *

Scott Wallace,† Dan Dill,‡ and J. L. Dehmer

Calculations of core and valence level photoionization spectra of NO are presented and compared with available experimental data. A low-lying continuum shape resonance is identified in the σ photoionization channel, which is the analog of similar states found in other first-row diatomic molecules. Both partial cross sections and photoelectron angular distributions are discussed, and the effect of nuclear motion on these observables is treated. As an example, the partial cross section and photoelectron asymmetry parameter for the 5σ orbital is given in Figures 1 and 2.

Reference

[1]S. H. Southworth, C. M. Truesdale, P. Kobrin, D. Lindle, and D. A. Shirley, to be published.

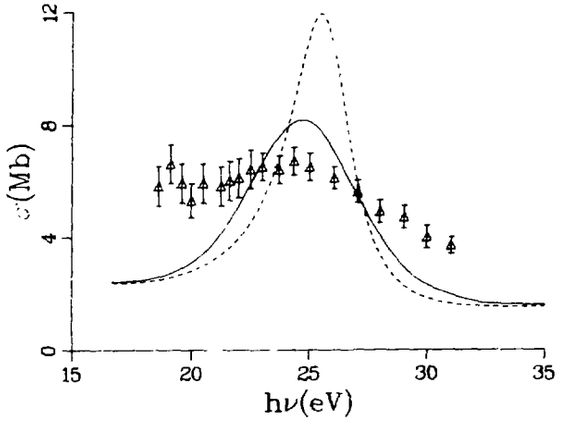

FIG. 1.--$NO^+ b^3\pi(5\sigma^{-1})$ cross section. Dashed line is for fixed-R, equilibrium internuclear separation; solid line has been averaged over nuclear motion. Data are from Ref. 1.

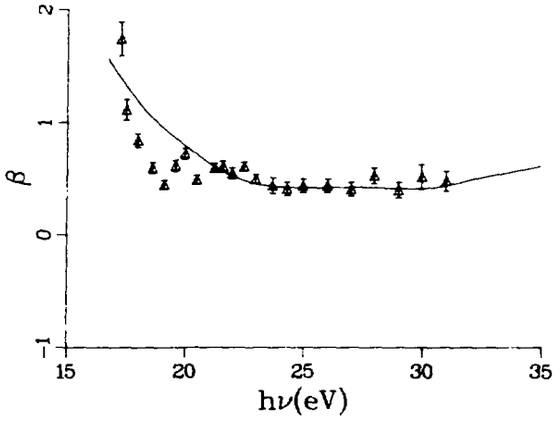

FIG. 2.--$NO^+ b^3\pi(5\sigma^{-1})$ asymmetry parameter. Calculations were averaged over nuclear motion. Data are from Ref. 1.

*Summary of a paper accepted for publication in J. Chem. Phys.

†Department of Materials Science and Engineering, Massachusetts Institute of Technology, Cambridge, MA 02139.

‡Consultant, Radiological and Environmental Research Division. Permanent address: Department of Chemistry, Boston University, Boston, MA 02215.

VIBRATIONAL EFFECTS IN THE SHAPE-RESONANT PHOTOIONIZATION OF CO_2*

J. R. Swanson,† Dan Dill,†‡ and J. L. Dehmer

Theoretical studies of several diatomic molecules predict that photoionization cross sections and angular distribution in spectral regions near shape resonances are very sensitive functions of nuclear separation.[1-3] This sensitivity is manifested in vibrationally unresolved cross sections σ and asymmetry parameters β by a broadening of resonant features relative to their fixed-nuclei profiles calculated at the equilibrium geometry. For vibrationally resolved spectra, the calculations predict large deviations from Franck-Condon vibrational intensity distributions and a strong dependence of β on the vibrational state of the residual ion. These predictions are supported by measurements of vibrational branching ratios and vibrationally resolved asymmetry parameters for the photoionization of the 5σ level of CO[4,5] and of the $3\sigma_g$ level of N_2.[6-11]

In a recent letter[12] we presented vibrationally averaged (i.e., unresolved) cross sections for the $1\pi_g$ and $4\sigma_g$ levels of CO_2. Both levels access the σ_u shape resonance which occurs at electron kinetic energy 19 eV. As was the case for the diatomics, the effect of averaging was to broaden and diminish the resonant cross section. The intensity of the resonance was reduced 70% in the $4\sigma_g$ channel and was left barely discernible in the $1\pi_g$ channel. Those results are complemented here by vibrationally averaged β's for the $1\pi_g$, $1\pi_u$, $3\sigma_u$, and $4\sigma_g$ levels, and by vibrationally resolved β's and vibrational branching ratios for the $1\pi_g$ and $1\pi_u$ levels. The vibrationally resolved results are shown in Figures 1 and 2 as examples. Vibrational parameters for the states resulting from ionization of the $3\sigma_u$ and $4\sigma_g$ levels were not available. However, we anticipate a prominent vibrational dependence in these channels owing to the σ_g and σ_u shape resonances. The averaged β's are in good agreement with recent synchrotron measurements.[14] The vibrationally resolved β's are in qualitative agreement with the recent He(I) line-source measurements of Kreile and Schweig.[13]

---

*Summary of a paper published in J. Phys. B 14, L207 (1981).
†Department of Chemistry, Boston University, Boston, MA 02215.
‡Consultant, Radiological and Environmental Research Division.

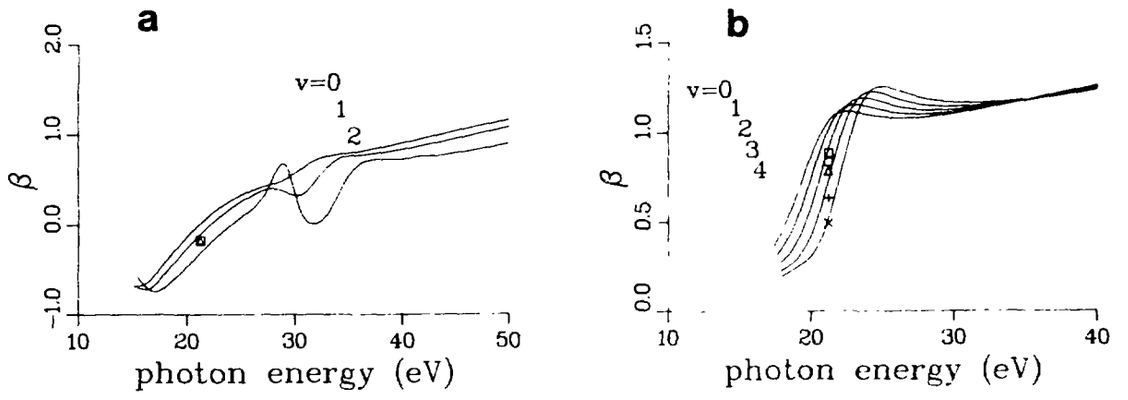

FIG. 1.--Vibrationally resolved asymmetry parameters of CO_2 for the (a) $1\pi_g$ level (□, v = 0; Δ, v = 1) and the (b) $1\pi_u$ level (□, v = 0; ○, v = 1; Δ, v = 2; +, v = 3; x, v = 4). The He(I) line-source data are from Kreile and Schweig.[13]

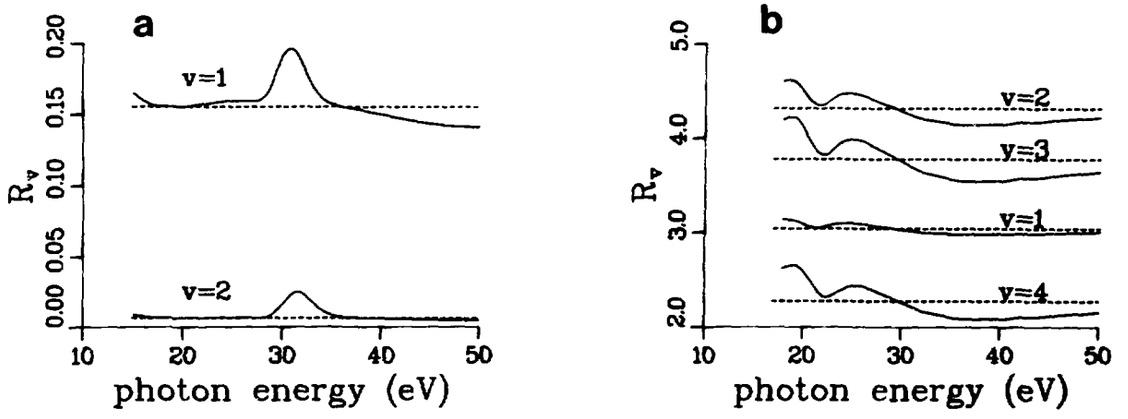

FIG. 2.--Vibrational branching ratios for the (a) $1\pi_g$ and (b) $1\pi_u$ levels of CO_2. The dashed lines represent the Franck-Condon branching ratios.

References

1. J. L. Dehmer, D. Dill, and S. Wallace, Phys. Rev. Lett. 43, 1005 (1979).
2. J. Stephens, D. Dill, and J. L. Dehmer, J. Phys. B., to be published.
3. P. Dittman, D. Dill, and J. L. Dehmer, J. Chem. Phys., to be published.
4. R. Stockbauer, B. E. Cole, D. L. Ederer, J. B. West, A. C. Parr, and J. L. Dehmer, Phys. Rev. Lett. 43, 757 (1979).
5. B. E. Cole, D. L. Ederer, R. Stockbauer, K. Codling, A. C. Parr, J. B. West, E. D. Poliakoff, and J. L. Dehmer, J. Chem. Phys. 72, 6308 (1980).
6. J. B. West, A. C. Parr, B. E. Cole, D. L. Ederer, R. Stockbauer, and J. L. Dehmer, J. Phys. B 13, L105 (1980).
7. T. A. Carlson, Chem. Phys. Lett. 9, 23 (1971).
8. T. A. Carlson and A. E. Jonas, J. Chem. Phys. 55, 4913 (1971).
9. D. M. Mintz and A. Kuppermann, J. Chem. Phys. 59, 3933 (1978).
10. W. H. Hancock and J.A.R. Samson, J. Electron Spectrosc. 9, 211 (1976).
11. T. A. Carlson, M. O. Krause, D. Mehaffy, J. W. Taylor, F. A. Grimm, and J. D. Allen, J. Chem. Phys. 73, 6056 (1980).
12. J. R. Swanson, D. Dill, and J. L. Dehmer, J. Phys. B 13, L231 (1980).
13. J. Kreile and A. Schweig, J. Electron Spectrosc. 20, 191 (1980).
14. F. A. Grimm, J. D. Allen, Jr., T. A. Carlson, M. O. Krause, D. Mehaffy, P. R. Keller, and J. W. Taylor, J. Chem. Phys. 75, 92 (1981).

SHAPE-RESONANCE EFFECTS IN THE PHOTOABSORPTION SPECTRA OF BF_3 *

J. R. Swanson,† Dan Dill,†‡ and J. L. Dehmer

Multiple-scattering model calculations of cross sections for dipole transitions from all occupied orbitals of BF_3 to excited bound states and continuum states of electron kinetic energy < 30 eV are presented. The photoelectron angular distribution asymmetry parameters β are also given for all occupied orbitals. The boron and fluorine K-shell calculations are in qualitative agreement with, and provide a clear interpretation of, the measured spectra. Two shape resonances are found in the low energy continuum, one of a_1' symmetry, the other of e' symmetry. The resonances are found to be due to trapping of p waves on the fluorine atoms. This atomic localization, as well as the dominance of low-ℓ partial waves outside the molecule, put these shape resonances in a class distinct from those observed in diatomic molecules. The results for the 2e' orbital of BF_3 (IP ∿ 2.3 Ry) are given in Figure 1 as an example. Both the a_1' and e' shape resonances are clearly shown at hν-IP ∿ 7 to 8 eV.

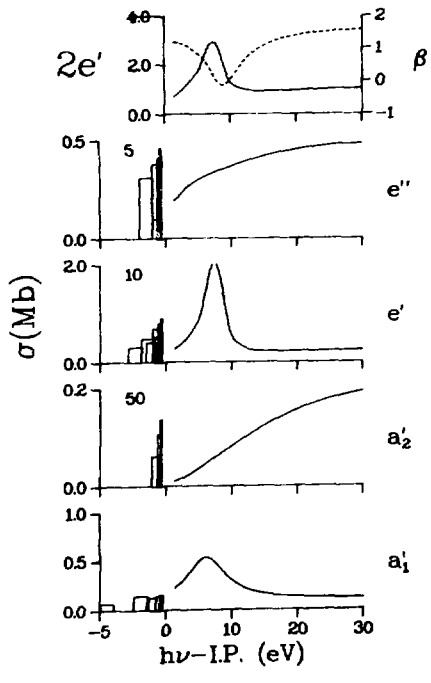

FIG. 1.--Partial cross sections and photoelectron asymmetry parameter for the 2e' subshell of BF_3. The lower subplots display partial cross sections; the upper subplots show the total cross section (solid lines—left scale) and asymmetry parameter (dashed lines—right scale). Note that the energy scale is expanded for E < 0. The factor above the discrete spectra indicates that the whole discrete spectrum has been multiplied by that factor.

---

*Summary of an article to appear in J. Chem. Phys.

†Department of Chemistry, Boston University, Boston, MA 02215.
‡Consultant, Radiological and Environmental Research Division.

MULTIPHOTON PROCESSES IN ATOMS AND MOLECULES

J. L. Dehmer, P. M. Dehmer, and E. D. Poliakoff

We have initiated a new program of laboratory studies of multiphoton processes in atoms and molecules involving observation of the fluorescence, photoelectrons, and/or molecular fragments produced by laser excitation. Emphasis will be placed on establishing the high-resolution spectroscopy and detailed dynamics of each successive step of the multiphoton process. Special attention will be given to sequences of resonant steps, excited by laser beams of different frequencies and polarization. Such a sequence is well-defined, highly selective, and very efficient at low power levels. To implement this program, we have recently finished assembling a unique combination of state-of-the-art instrumentation. This includes: (1) a high-power pulsed Nd:YAG laser and companion commercial dye laser with nonlinear conversion capabilities, (2) a detailed design (provided by F. Tomkins, Chemistry Division) for a two-grating, Littman-mount dye laser, several of which will be constructed at ANL for use in multicolor experiments, (3) a high-resolution electron spectrometer, (4) a time-of-flight mass spectrometer, (5) a fluorescence detector including capabilities for measuring the polarization of fluorescence, and (6) an assortment of molecular beam sources for studying rotationally-cooled species, clusters, free radicals, and high-temperature vapors.

The multiphoton studies described here will exploit a number of special features of excitation by pulsed lasers. First, using standard line-narrowing techniques, very high resolution is attainable (the pump and dye laser have limiting bandwidths of 0.01—0.05 cm^{-1}), permitting resolution of rovibronic structure for most molecules. Second, the tunability of dye lasers permits precise state selection of the target molecule in each excitation step. Third, the high photon flux of the pulsed laser system makes it possible for an isolated molecule to undergo successive excitations during a single laser pulse. Fourth, multiphoton processes can access manifolds of states forbidden by rigorous selection rules in single-photon absorption. Fifth, the high flux of the laser coupled with the high selectivity of resonant transitions makes multiphoton

processes capable of the ultimate sensitivity, i.e., ability to detect reactive, unstable, or trace species, even in the presence of large amounts of other species. Sixth, the high photon flux and uniphase character of the dye laser output permits frequency conversion by means of doubling, summing, coherent anti-Stokes shifting, four-wave mixing, etc. This allows shifting the tunable laser frequencies into the UV so that high energy transitions (usually the lowest electronic excitations of a molecule) can be pumped by a single photon. Seventh, the energy content of the pulses from our Nd:YAG pump laser makes it possible to pump many dye lasers simultaneously. This permits preparation of a composite laser beam composed of component beams of selected frequency, polarization state, and flux. This "multicolor" beam can be specially designed to probe a particular sequence of state-to-state resonant transitions in a target molecule and to observe the spectroscopy of any stage in the excitation process by tuning one of the component frequencies.

This program aims at providing the requisite research to develop ultrasensitive detection schemes for atmospheric species. In particular, the combination of the highly selective excitation mechanism and the additional detection stages indicated above have the porential for (a) ultrasensitive detection far behond the currently attainable level of parts per billion toward the ultimate limit of single-molecule detection (1 part in 10^{19}); (b) chemical specificity. including the ability to distinguish chemically similar molecules and the detection of internal excitation; (c) direct monitoring, which eliminates the need for sample handling and thus permits the study of chemically reactive and loosely bound species.

Preliminary measurements are scheduled to begin in the spring of 1981.

A NEW OPTICALLY-FORBIDDEN RYDBERG SERIES IN O_2 CONVERGING TO THE $O_2^+ c^4\Sigma_u^-$ LIMIT *

M. A. Dillon and David Spence

We have measured the angular dependence of inelastically scattered electrons in O_2 in the energy-loss range 16 to 26 eV for incident electron energies between 75 eV and 400 eV, and for scattering angles between 2° and 12°. For high incident energy and low scattering angle our energy-loss spectra correspond to the known optical absorption spectrum. At higher scattering angles four new structures appear in our spectra at 21.85, 23.30, 23.80, and 24.06 eV. These four structures are the lowest members of the first optically forbidden Rydberg series observed to converge to the $O_2^+ c^4\Sigma_u^-$ limit at 24.56 eV. The calculated quantum defects for these levels are about 0.75. This value, combined with angular scattering propensity rules, indicates that the new Rydberg states occur by promotion of an electron from the $\sigma_u 2s$ orbital to $np\sigma_u$ orbitals where n = 3, 4, 5, 6. A consideration of the propensity rules for excitation of forbidden transitions by high energy electron impact suggests the term symbol of the new Rydberg states to be $^3\Sigma_g$.

*Abstract of a paper to appear in J. Chem. Phys.

THE ANGULAR DEPENDENCE OF SCATTERED ELECTRON SPECTRA OF NEON AND ARGON IN THE REGION OF QUASI-DISCRETE AUTOIONIZING STATES*

M. A. Dillon and David Spence

We have measured the angular dependence of inelastically scattered electrons in neon and argon in the energy region of quasi-discrete autoionizing states. Our spectra, obtained for incident electron energies of 200 eV, show that both singly and doubly excited autoionizing states exhibit angular distributions of the scattered electrons which are qualitatively as predicted by the Born approximation. Our results demonstrate that measured angular distributions of electrons scattered from quasi-discrete states can yield information on the symmetries and term symbols of these states, in a manner analogous to the well-known propensity rules for excitation of bound states.

---

*Abstract of a paper published in J. Chem. Phys. 74, 2654 (1981).

STUDIES OF THE O_2 $^3\Pi_g(V)$ VALENCE STATE AND $^3\Pi_g(R)$ RYDBERG STATE IN THE SCHUMANN-RUNGE CONTINUUM FROM EJECTED AND SCATTERED ELECTRON SPECTRA†

David Spence

Electron-impact energy-loss spectra are obtained in O_2 in the energy-loss range of 7 to 10 eV. These spectra contain some discrete features resulting from scattered electrons following excitation of Rydberg states, and other features from ejected electrons following decay of O_2^{-*} Feshbach resonances into valence electronic states in the continuum via the reaction $e + O_2 (X\ ^3\Sigma_g^-) \rightarrow (O_2^{-*}) \rightarrow O_2\ ^3\Pi_g(V) + e_{ejected}$. From the known O_2^{-*} energies and from measurements of the ejected electron energies, we find the $^3\Pi_g(V)$ state extends over an energy range of only about 0.20 eV in the Franck-Condon region of the ground state, contrary to some previous experimental and theoretical results. From measurements of scattered electrons, effective excitation functions of several vibrational levels of the $^3\Pi_g$ (R) Rydberg state are obtained. Of the many O_2^{-*} Feshbach resonances known to exist in this energy region, only one decays strongly into the $^3\Pi_g(R)$ state.

---

†Abstract of a paper published in J. Chem. Phys. 74, 3898 (1981).

ON RESONANCES IN HF*

David Spence

We discuss a probable explanation of the totally inconsistent nature of some previously published Feshbach resonance spectra of hydrogen fluoride which has been provided by the recent work of Brion and Hitchcock.[1] We have obtained new electron transmission spectra of HF in the energy range 12.8 to 16.0 eV, which confirm the earlier HF resonance data of Spence and Noguchi[2] and which reveal several previously unobserved resonance structures. These new structures are energetically coincident with the higher lying members of a series of peaks recently found in the F^-/HF dissociative attachment cross section. We explain the anomalous scattering from the $HF^{-2}\Pi(v = 0)$ resonance level in terms of the mixing of the $b\ ^3\Pi$ and $B\ ^1\Sigma$ parent Rydberg states which has been observed in optical absorption spectra. Finally, we point out a possible mechanism for a Lyman-α laser.

References

1. C. E. Brion and A. P. Hitchcock, J. Phys. B, in press.
2. D. Spence and T. Noguchi, J. Chem. Phys. 63, 505-514 (1975).

---

*Abstract of a paper published in J. Phys. B 14, L107 (1981).

ENERGY LEVELS AND PREDISSOCIATION IN MERCURIC HALIDES

David Spence and Michael A. Dillon

In recent years the mercuric halides have attracted considerable interest as potential high-power electronic transition laser systems.[1-3] Though the mercuric halides have been studied for a hundred years by photoabsorption and emission techniques,[4] only the energetically lowest-lying electronic states have been cataloged. Because the symmetries and electronic structure of the excited states of HgX_2 are not known, the detailed nature of the laser mechanism in the mercuric halides is incompletely understood. Although the principal laser mechanism is believed to be

$$HgX_2(1^1\Sigma_g^+) \xrightarrow{h\nu} HgX_2(^1\Sigma_u^+) \rightarrow HgX_2(B^2\Sigma^+) + X(^2P) \quad ,$$

followed by

$$HgX(B^2\Sigma^+) \rightarrow HgX(X^2\Sigma^+) + h\nu \quad ,$$

the $1^1\Sigma_u^+$ states of HgX_2 occur at a lower energy[4] than the apparent onset of fluorescence radiation[5] upon electron impact excitation of HgX_2. This suggests that states higher in energy than $1^1\Sigma_u^+$ may also play some role in the laser mechanism. For example, it is feasible that some higher-lying excited states of HgX_2 may predissociate into the products $HgX(B^2\Sigma^+) + X(^2P)$.

For these reasons we have obtained electron energy-loss spectra over an extended energy-loss range (approximately 5 to 15 eV) for incident electron energies of 200 eV and scattering angles of 2° in the mercuric halides $HgBr_2$ and $HgCl_2$. Under these conditions of impact energy and scattering angle, the energy-loss spectra correspond closely to optical absorption spectra,[6] though our energy-loss spectra extend to much higher energies than previous photoabsorption spectra, and reveal many more excited states of these molecules than had previously been observed.

Although analysis of our data is not yet complete, we will, in this preliminary report, give our raw spectra and tentative identifications of the principal features of these spectra.

Results

Electron energy-loss spectra in $HgCl_2$ and $HgBr_2$ are shown in Figures 1 and 2, respectively. The locations of three dipole-allowed transitions, $1\,^1\Pi_u$, $1\,^1\Sigma_u^+$, and $2\,^1\Sigma_u^+$, which have been observed in photoabsorption[7-9] and calculated theoretically[4] are indicated by the short vertical lines. All of these three features occur as broad structures in optical absorption spectra, and the $1\,^1\Pi_u$ transition is barely discernible in Figures 1 and 2 here.

All the structures above about 8 eV correspond to electronic energy levels not previously observed, the most prominent of these structures corresponding to transitions to Rydberg states, as is usually the case for energy-loss spectra taken for incident energies of 200 eV.

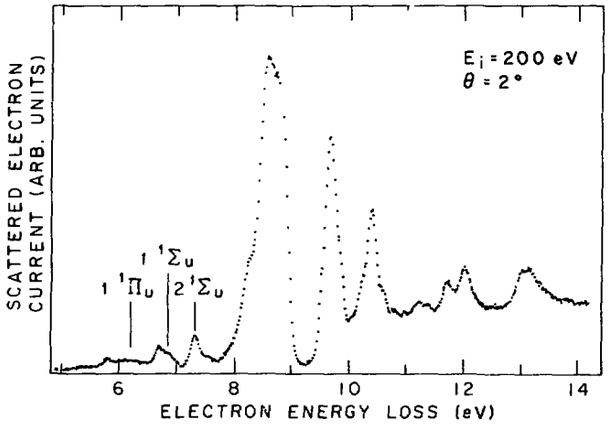

FIG. 1.--Electron energy-loss spectrum in $HgCl_2$.

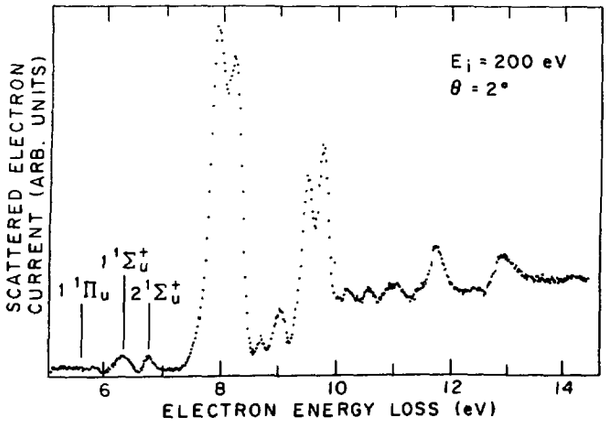

FIG. 2.--Electron energy-loss spectrum in $HgBr_2$.

Interpretation of the most prominent structures in Figures 1 and 2 is facilitated with reference to the photoelectron spectra of $HgCl_2$ ahd $HgBr_2$ obtained by Eland.[10] The photoelectron spectra of Eland correspond to removing an electron from different valence orbitals, leaving an ion in either its ground or excited state. The spectra of Rydberg states in the energy-loss spectra of Figures 1 and 2 correspond to exciting an electron from these same initial orbitals to Rydberg orbitals.

Rydberg orbitals are essentially nonbonding, and hence in general electron energy-loss Rydberg state spectra usually look very similar to photoelectron spectra. Comparison of Figure 1 with the photoelectron spectrum of $HgCl_2$ shows this indeed to be the case. The five lowest structures in the photoelectron spectrum correspond to removing electrons from π_g, π_u, σ_u, and σ_g orbitals, leaving the ion in the respective ionic states $^2\Pi_{3/2g}$, $^2\Pi_{1/2g}$, $^2\Pi_{3/2,1/2u}$ (unresolved), $^2\Sigma_u$ and $^2\Sigma_g$.

The prominent structures in Figures 1 and 2 thus correspond to excited states composed of an ionic core with term symbols listed above and an electron in a Rydberg orbital. The symmetries of the Rydberg orbitals can be tentatively assigned from a knowledge of the Rydberg state quantum defects, which can be obtained from the Rydberg formula

$$E_{n\ell} = I = RZ^2/(n-\delta_{n\ell})^2 \quad ,$$

where $E_{n\ell}$ is the Rydberg state energy, I the appropriate ionization potential, R the Rydberg constant, Z the nuclear charge, n the principal quantum number of the Rydberg orbital, and $\delta_{n\ell}$ the quantum defect of that orbital. Lindholm[11] has shown how orbital symmetries of simple molecules can be determined from the quantum defects. In Table 1, we list for $HgCl_2$ the <u>initial</u> orbitals, excited state energies $E_{n\ell}$ from Figure 1, the appropriate ionization potentials I from Eland,[10] effective quantum number n*, quantum defect $\delta_{n\ell}$ and <u>tentative</u> excited orbital symmetry.

The close visual similarity observed in the energy loss and photoelectron[10] spectrum of $HgCl_2$ is not so obvious in the case of $HgBr_2$. As one expects occupation of similar orbitals for excitation of $HgCl_2$ and $HgBr_2$, the quantum

Table 1. Observed excited state energies $E_{n\ell}$ and tentative excited state symmetries in $HgCl_2$.

Initial orbital	Excited state energy $E_{n\ell}$, eV	Ionization potential I, eV[10]	n*	$\delta_{n\ell}$	Excited orbital symmetry
π_g	8.60	11.37 $^2\Pi_{3/2g}$	2.22	0.78	npσ
π_g	8.73	11.50 $^2\Pi_{1/2g}$	2.22	0.78	
π_u	9.65	12.13 $^2\Pi_{3/2,1/2u}$	2.34	0.66	npπ
σ_u	10.40	12.74 $^2\Sigma_u$	2.41	0.59	npπ
σ_g	12.0	13.74 $^2\Sigma_g$	2.80	0.2	ndσ

defects of these orbitals in $HgBr_2$ must be similar to those in $HgCl_2$. Because of this, we are unable to assign one peak in the $HgBr_2$ spectrum, i.e., that at 9.48 eV which appears to be the lower member of a doublet structure (the splitting being approximately that of the $HgBr_2^+$ $^2\Pi_{3/2,1/2g}$ state). However, because of its similarity to $HgCl_2$, this peak cannot be a doublet associated with the $^2\Pi_u$ ionic state, but may contain components of the n = 4 $^2\Pi_g$ npσ structures. Furthermore, the similarity of the intensity ratios for energy-loss and photoelectron spectra in $HgBr_2$ do not hold so well in the case for $HgBr_2$ as in $HgCl_2$. For these reasons, the orbital assignments to $HgBr_2$ shown in Table 2 must be considered extremely tentative. However, the expected close similarities of quantum defects in $HgCl_2$ and $HgBr_2$ shown in Tables 1 and 2 do lend support to our interpretation.

In addition, one should note that all the structures in Figures 1 and 2 are rather broad energetically, being at least 0.2 eV for the sharpest structure. This is not a reflection of our instrumental resolution which is better than 0.05 eV as determined from energy-loss spectra obtained in argon while running Ar-$HgCl_2$, Ar-$HgBr_2$ mixtures. Furthermore, the photoelectron spectra[10] of $HgCl_2$ and $HgBr_2$ show $^2\Pi_{3/2,1/2g}$ structures which reflect the instrumental width of $\sim$ 0.1 eV.[10] Thus, either all the potential curves of the excited states

Table 2. Observed excited state energies $E_{n\lambda}$ and tentative excited state symmetries in $HgBr_2$.

Initial orbital	Excited state energy $E_{n\lambda}$, eV	Ionization potential I, eV[10]	n*	$\delta_{n\lambda}$	Excited orbital symmetry
π_g	7.9	10.62 $^2\Pi_{3/2g}$	2.24	0.76	} np
π_g	8.19	10.96 $^2\Pi_{1/2g}$	2.22	0.78	}
π_u	8.71	11.20 $^2\Pi_{3/2u}$	2.34	0.66	} npπ
π_u	9.03	11.54 $^2\Pi_{1/2u}$	2.33	0.67	}
	9.48	? ?			
σ_u	9.76	12.09 $^2\Sigma_u$	2.42	0.59	npπ
σ_u	11.75	13.39 $^2\Sigma_g$	2.88	0.12	ndσ

indicated by the structures of Figures 1 and 2 are repulsive in the Franck-Condon region of the ground state, or the states predissociate. A simple observation of a finite width to a state indicates its quantum yield for predissociation to be unity.

For reasons listed above, prime candidates for such a predissociating state appear to be the ($^2\Pi_{3/2,1/2g}$) npσ Rydberg states listed in Tables 1 and 2. Note that these states occur at an energy close to the observed onset of fluorescence upon electron impact,[5] and that the fluorescence yield curves as a function of incident electron energy correspond to that expected for excitation of Rydberg states. Thus, it is possible that some of these higher excited states may be predissociating to the products $HgX(B\,^2\Sigma^+) + X(^2P)$ and thus contributing to the laser mechanism.

Finally, one should note that multiplication of the intensity of scattered electrons in Figures 1 and 2 by the energy-loss E gives the generalized oscillator strength distribution. It is clear that most of this oscillator strength lies above the three lowest indicated dipole-allowed transitions.

References

1. J. H. Parkes, Appl. Phys. Lett. 31, 192 (1977).
2. J. H. Parkes, Appl. Phys. Lett. 31, 297 (1977).
3. J. H. Jacob, J. A. Mangano, M. Rokni, and B. Srivastava, Bull. Am. Phys. Soc. 23, 2 (1976).
4. W. R. Wadt, J. Chem. Phys. 72, 2469 (1980) and references therein.
5. J. Allison and R. N. Zare, Chem. Phys. 38, 263 (1978).
6. R. A. Dillon and S. Spence, J. Chem. Phys., in press.
7. J. Maya, J. Chem. Phys. 67, 4976 (1977).
8. K. Wieland, Z. Phys. 76, 801 (1932); 77, 157 (1932).
9. M. Wehrli, Helv. Phys. Acta 11, 339 (1938).
10. J.H.P. Eland, Int. J. Mass Spect. and Ion Phys. 4, 37 (1970).
11. E. Lindholm, Ark, Phys. 40, 97 (1969).

SEARCH FOR LONG-LIVED DOUBLY CHARGED ATOMIC NEGATIVE IONS*

D. Spence, W. A. Chupka,† and C. M. Stevens‡

In a previous brief report[1] we described our preliminary attempts to detect doubly charged atomic negative ions using the ANL 100" radius double-focussing mass spectrometer. Since that time, several other papers reporting both negative[2,3] and positive results[4] have appeared in the literature concerning the existence of long-lived doubly charged negative ions. A recent lengthy review article concludes that such ions definitely exist.[4] However, among the conflicting reports in the literature, only one negative experiment[2] has come close to reproducing the ion source conditions of those earlier experiments which have yielded positive results.[5] This aspect of any comparison between negative and positive reports on the existence of such ions is important, since ion species produced in an ion source depends crucially upon the type of ion source used, and upon source conditions such as gas pressure and electron or discharge currents.[6] For these reasons, and because of the technological importance of doubly charged ions if they exist, we describe in this report the results of our experimental search for doubly charged negative ions in considerable detail.

In all of our experiments we have used the Argonne 100" radius double-focussing mass spectrometer,[7,8] a schematic diagram of which is shown in Figure 1. The ultimate mass resolution of this machine is of the order 10^6, and it was, in fact, designed for precision absolute mass measurements. Such high resolution is not required in the present experiments, and we have typically operated at a mass resolution of 2×10^3 to 1.5×10^4, under which conditions the transmission of the mass spectrometer is about 95%.

An important feature of this machine is that artifact peaks (caused, for example, by collisional dissociation of diatomic ions with the background gas

---

*Summary of a paper to appear in Phys. Rev. A.

†Present address: Stirling Chemical Laboratories, Yale University, New Haven, Connecticut 06520.

‡ANL Chemistry Division.

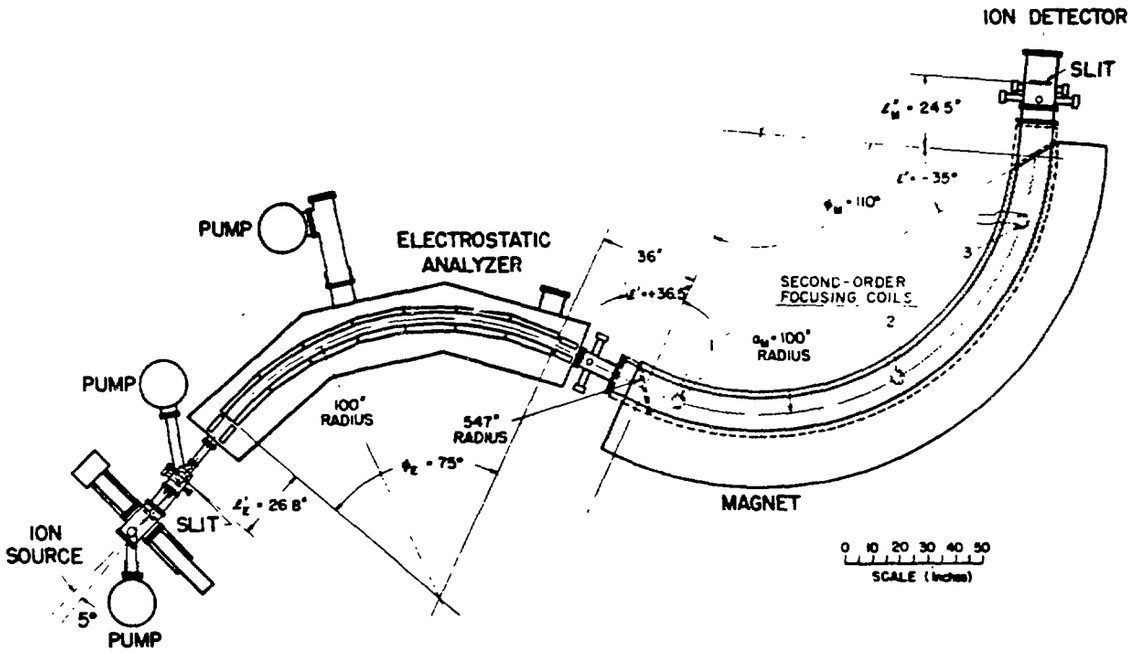

FIG. 1.--Schematic diagram of the ANL 100" radius double focussing mass spectrometer

to yield an atomic ion plus neutral) do not occur. Such artifact peaks, known as Aston peaks, if caused by dissociation of a molecular ion after acceleration but before mass analysis in a magnetic sector, will occur at an apparent mass of half that of an atomic ion, i.e., at the expected location of a doubly charged negative ion. In some previous experiments Aston peaks have complicated interpretation of the results.[2,3,5] In our machine the focussing conditions and background gas pressure between the electrostatic analyzer and magnetic analyzer are such that artifact peaks do not occur, as we will demonstrate later.

In our experiments we have used both electron-impact and Penning ionization type sources in order to duplicate as closely as possible previous experimental conditions which do report the existence of doubly charged ions.[5,9,10] Our conditions of flight time and electric field strengths during acceleration do not differ enough from those of earlier work[5] to be significant in the interpretation of our results.

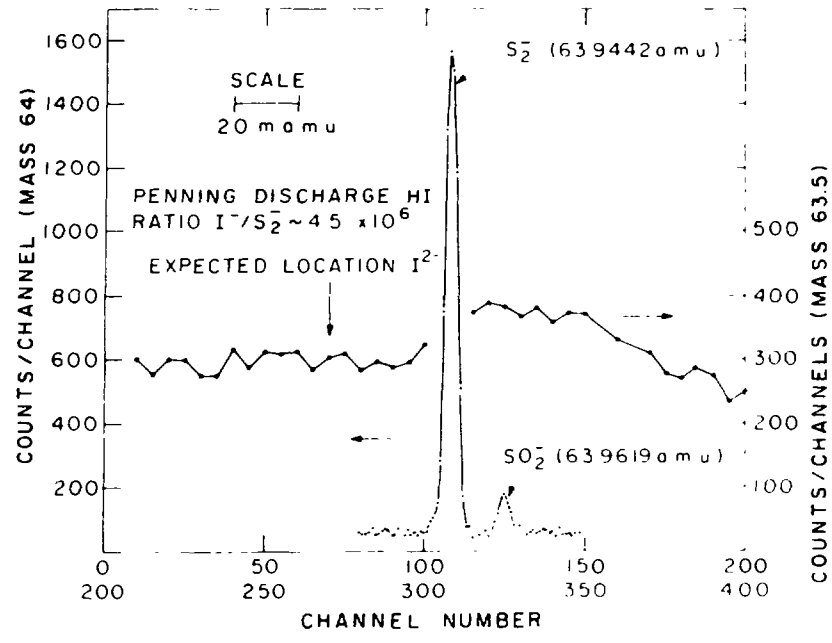

FIG. 2.--Mass spectra of negative ions produced in a Penning ionization source containing HI in the region of mass 64 (SO_2^- and S_2^- produced from background impurities, channels 200 → 400) and in the mass region any I^{2-} would be expected to appear (mass 63.5, channels 0 → 200). From the ratio of I^{2-}/SO_2^- and SO_2^-/I^- measured in an electrometer, we set limits of $I^{2-}/I^- \leq 4.5 \times 10^{-10}$ in this experiment. Note our resolution is such that 200 channels correspond correspond to approximately 200 millimass units (m.a.m.j.), i.e., $\Delta m/m \sim 12{,}800$.

We present results of our experiments as an upper limit of the ratio of doubly charged to singly charged species, X^{2-}/X^- for different ion sources, target gases, and negative ion species. However, the sensitivity of our machine is such that this ratio is very small, typically 10^{-7} to 10^{-10}, and is obtained in two stages as described below. First, we choose an arbitrary negative ion Y^- (generated from impurities in the ion source region, the sensitivity being such that an ion can be observed at most mass numbers) whose mass lies close to that of the expected doubly charged species. The intensity of this arbitrary ion is necessarily small, but sufficiently large to measure on the output of a photomultiplier with an electrometer. The ratio Y^-/X^- is measured on the electrometers. Then, with operation in a pulse counting mode, multiple alternate scans of Y^- and possible X^{2-} are stored in a multichannel analyzer. The ratio X^{2-}/Y^- is then obtained and hence X^{2-}/X^-.

An example of such a scan is shown in Figure 2 where channels 0 to 200 show the mass spectrum around mass 63.5, the expected location of I^{2-}, and channels 200 to 400 show a mass scan around 64 (SO_2^- and S_2^-). Note SO_2 and S_2 have nominally the same mass, separated by only 18 millimass units. Our mass scale can be set to 1 millimass unit which, combined with our resolution, gives us a positive identification of any ion we observe. Previous experiments[2,5] have not had such high resolution and thus, although one experiment[2] has determined that a previous observation[5] of an ion at 63.5 is not I^-, but rather some impurity, the resolution[2] was insufficient to determine what this impurity may be.

Table 1. Electron Impact Ionization Source

Target gas	Ratio X^{2-}/X^- from previous data	Ratio X^{2-}/X^- from present data
CF_3I		$I^{2-}/I^- \leq 1.3 \times 10^{-7}$
CF_3I		$F^{2-}/F^- \leq 2.1 \times 10^{-7}$
CF_3Cl	$F^2/F^- \approx 10^{-1}$, a,b	$F^{2-}/F^- \leq 4.6 \times 10^{-8}$
CF_3Cl	$Cl^{2-}/Cl^- \approx 10^{-1}$, a	$Cl^{2-}/Cl^- \leq 1.15 \times 10^{-7}$
O_2	$O^{2-}/O^- \approx 10^{-3} \rightarrow 10^{-14}$, c	$O^{2-}/O^- \leq 1.0 \times 10^{-7}$
CCl_4		$Cl^{2-}/Cl^- \leq 2.0 \times 10^{-8}$
I_2		$I^{2-}/I^- \leq 1.0 \times 10^{-8}$
	Penning Ionization Source	
HI		
I_2	$I^{2-}/I^- \approx 10^{-3}$, c	$I^{2-}/I^- \leq 5.0 \times 10^{-10}$
$H_2 + I_2$		

[a] Ref. 9.

[b] Ref. 10.

[c] Ref. 5.

It is obvious from Figure 2 that no ions are detectable above noise in the region of mass 63.5. This figure also demonstrates the lack of any Aston peaks in our apparatus as our ion source certainly produces copious quantities of I^{2-} from Figure 2 and electrometer measurements of I^-/SO_2^-, we can establish limits of $I^=/I^-$ produced in a Penning discharge in HI to be $< 4.5 \times 10^{-10}$ in this particular experiment.

The results of most of our experiments, using both electron impact and Penning ionization sources, together with source conditions, are summarized in Table 1. Under no experimental conditions did we detect any indication of a doubly charged atomic negative ion. Thus, in light of this and other negative experiments,[2,3] it appears at this time that any evidence supporting the existence of doubly charged negative ions be considered extremely tenuous.

References

1. W. A. Chupka, D. Spence, and C. M. Stevens, Radiological and Environmental Research Division Annual Report, July 1973-June 1974, ANL-75-3, Part I, p. 126.
2. L. Frees, E. Heinicke, and W. S. Koski, Mucl. Instrum. Methods 159, 105 (1979).
3. B. Hird and S. P. Ali, J. Chem. Phys. 74, 3620 (1981).
4. R. W. Kiser, Topics in Curr. Chem. 85, 89 (1979).
5. H. Baumann, E. Hienicke, H. J. Kaiser, and K. Bethge, Nucl. Instrum. Methods 95, 389 (1971).
6. R. D. Mead, P. A. Schulz, C. S. Feigerle, and W. C. Lineberger, IEEE Trans. Nucl. Sci. 28, NS-1194 (1981).
7. C. M. Stevens, J. Teranay, G. Lobell, J. Wolfe, N. Beyer, and R. Lewis, Proc. 9th Conf. on Nuclidic Masses, Hamilton, Ont., p. 403 (1960).
8. C. M. Stevens and P. E. Moreland, Proc. Third Int. Conf. on Atomic Masses, Winnipeg, Canada, p. 673 (1967).
9. W. K. Stuckey and R. W. Kiser, Nature 211, 963 (1960).
10. J. E. Ahnell and W. S. Koski, Nature 245, 30 (1973).

DOUBLY-DIFFERENTIAL CROSS SECTIONS OF SECONDARY ELECTRONS EJECTED FROM GASES BY ELECTRON IMPACT: 25–250 eV ON H_2.*

W. T. Shyn,† W. E. Sharp,† and Y.-K. Kim

Doubly-differential cross sections of secondary electrons ejected from H_2 by electron impact have been measured by a crossed-beam method. The incident energies used were 25, 40, 60, 100, 150, and 250 eV. The energy and angular range of secondary electrons measured were from one-half the difference between incident energy and ionization potential to 1.0 eV and from 12° to 156°, respectively. The present results do not agree with those of DuBois and Rudd[1] for slow secondary electrons (< 20 eV) ejected by 100 eV primary electrons.

We present our data in Figure 1 as the Platzman plot.[2] The data by Opal, Beaty, and Peterson[3] at 500 eV incident energy, E_i, and our data at E_i = 250 eV are compared with the shape of the corresponding photoionization data[4,5] again in the Platzman plot (Figure 2). The total ionization cross section, σ_i, obtained by integrating the energy distribution (area under the broken curves in Figure 2) by Opal et al.[3] is far too large. The H_2 data by Opal et al. should

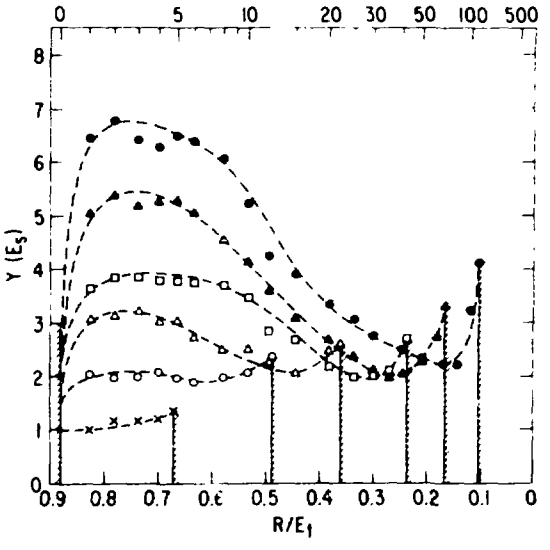

FIG. 1.--The Platzman plots of the present results at various incident energies, E_i. X, 25 eV; o, 40 eV; Δ, 60 eV; □, 100 eV; —, 150 eV; ●, 250 eV. The abscissa is the inverse of the energy transfer, E_t, in rydbergs, and the ordinate is the ratio of the energy distribution to the Rutherford cross section. Secondary electron energy scale is on the top. Area under each Platzman plot bounded by the hatched lines gives the total ionization cross section, σ_i, as explained in Ref. 2. Broken curves were used to obtain σ_i from our data.

---

*Summary of a paper published in Phys. Rev. A 24, 79 (1981).

†Space Physics Research Laboratory, University of Michigan, Ann Arbor, Michigan 48109.

be reduced by one-third to be consistent with direct measurements[6,7] of σ_i. Our data lead to total ionization cross sections within 10% of other measurements.[3,4]

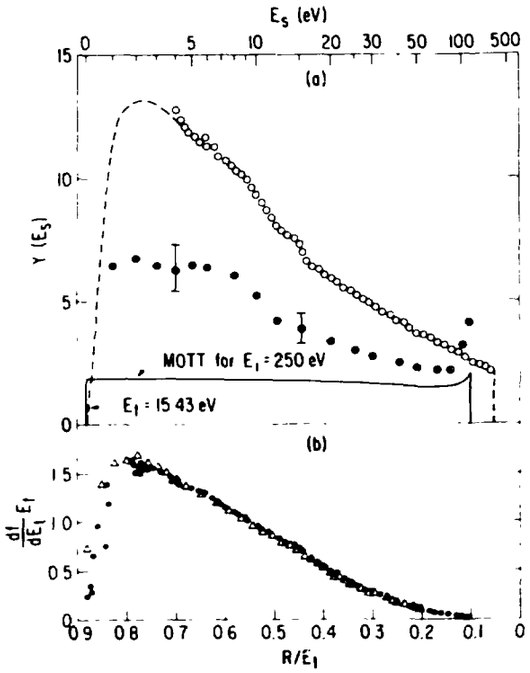

FIG. 2.--Comparison of secondary-electron energy distributions and photoionization cross sections of H_2. (a) The Platzman plot of electron-impact data by Opal, Beaty, and Peterson[3] (open circles) at 500 eV incident energy, and those by the present authors at 250 eV incident energy (solid circles). Energy transfer of 15.43 eV is the first ionization potential of H_2, corresponding to the production of zero-kinetic energy secondaries. The Mott cross section qualitatively represents that part of the ionization caused from knock-on (large momentum transfer) collisions. The broken curve was used in integrating the data by Opal et al. to obtain the total ionization cross section. (b) The continuum dipole oscillator strengths, df/dE_t, (E_t here is the photon energy) were derived from the photoionization measurement by Samson and Haddad (solid circles)[4] and from the electron-impact data by Backx, Wight, and van der Wiel (triangles).[5] The ordinate of (b) represents qualitatively the contribution of dipole-allowed interaction; the shape of the curve should be compared to that of the difference between the electron-impact data and the Mott cross section in (a)

References

1. R. D. DuBois and M. E. Rudd, Phys. Rev. A 17, 843 (1978).
2. Y.-K. Kim, Radiat. Res. 61, 21 (1975); 64, 205 (1975).
3. C. B. Opal, E. C. Beaty, and W. K. Peterson, Atom. Data 4, 209 (1972).
4. J.A.R. Samson and G. N. Haddad, personal communication [their data presented by J.A.R. Samson, Phys. Rev. 28C, 303 (1976), Fig. 9].
5. C. Backx, G. R. Wight and M. J. van der Wiel, J. Phys. B 9, 315 (1976).
6. J. T. Tate and P. T. Smith, Phys. Rev. 39, 270 (1932).
7. D. Rapp and P. Englander-Golden, J. Chem. Phys. 43, 1464 (1965).

CROSS SECTIONS FOR ELECTRON INELASTIC COLLISIONS WITH ARGON*

E. Eggarter† and Mitio Inokuti

We present in tabular form a complete set of optical oscillator strengths and electron-impact cross sections for the argon atom. A large variety of experimental data and theoretical calculations was studied, and various checks based on theory (including the constraint of sum rules) were critically performed. Data were analyzed mainly by a semiempirical method that stresses the close relation of photoabsorption with electron-atom collisions.

*A complete report of this work appears in Argonne Report ANL-80-58 (July 1980).

†Universidad Nacional de San Luis, Facultad de Ciencias Fisico, Matematicas y Naturales, Escuela de Fisica, Chacabuco y Pedernera, 5700 San Luis, Argentina.

SPECTRA OF THE OSCILLATOR STRENGTH FOR ATOMS, MOLECULES, AND SOLIDS

Mitio Inokuti

The spectral distribution of the dipole oscillator strength over the entire energy range is a basic electronic property of any given material; it characterizes the response of the material to a spatially uniform but time-dependent electric field. Thus, the distribution governs many physical phenomena such as absorption and dispersion of light and long-range interactions with a fast charged particle, and the van der Waals forces. Two recent decades have been notable progress in the understanding of the distribution and of the dynamics that govern it. The lecture illustrates some of the recent results selected from current topics of research; examples include the evaluation of the mean excitation energy for stopping power, a comprehensive study on metallic aluminum, and near-threshold structure of the K-shell spectra of atoms and molecules.

*Summary of an invited lecture presented at the Spring Meeting of the Danish Physical Society, Atomic Physics Section and Solid State Section, May 1980, Helsingør, Denmark. The author acknowledges Nordisk Institut for Teoretisk Atomfysik, Copenhagen, Denmark, for the Visiting Professorship that supported the sojourn from April to July 1980 at Odense University.

OSCILLATOR-STRENGTH MOMENTS, STOPPING POWERS, AND TOTAL INELASTIC-SCATTERING CROSS SECTIONS OF ALL ATOMS THROUGH STRONTIUM*

Mitio Inokuti, J. L. Dehmer, T. Baer,[†] and J. D. Hanson[‡]

Systematics of the atomic properties named in the title and of other related quantities have been comprehensively studied. Our calculations are based on a single-electron approximation using the Hartree-Slater central potential — a model that represents a reasonable compromise between two goals, namely, a realistic description of the major features of atomic dynamics and an economical computation necessary for a survey of many atoms. Our results not only quantify the general trends of the atomic properties as qualitatively expected from the periodic table, but also provide a sensible guide to experiment (on atoms for which no other data are available), to theory (for which we suggest several specific aims of more advanced analysis), and to applications including radiological physics and charged-particle microscopy.

Figures 1-3 show selected examples of our results. Figure 1 shows the mean excitation energy I in the Bethe stopping-power formula.[1,2] Our calculations explain the general trends of experimental data: The ratio I/Z, where Z is the atomic number, varies periodically with Z, reflecting the outer-shell structure; and the variations damp at high Z because outer-shell contributions become less and less important for higher and higher Z.

Figure 2 gives the total inelastic-scattering cross section σ_{tot} for 50-keV electrons. The cross section σ_{tot} for any fast charged particles depends on Z in roughly the same way, and the dependence on Z is important for many applications such as energy-deposition analysis in radiological physics and charged-particle microscopy. Here the prominent periodic variations are due primarily to the outer-shell structure .

---

*Summary of a paper published in Phys. Rev. A 23, 95 (1981).

[†]Present address: Joint Institute for Laboratory Astrophysics, University of Colorado, Boulder, Colorado 80309.

[‡]Present address: Department of Applied Physics, Cornell University, Ithaca, New York 14850.

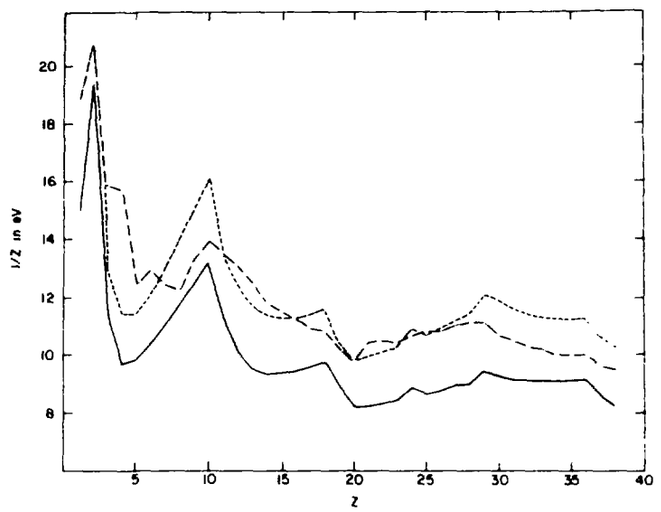

FIG. 1.--The mean excitation energy for stopping power per atomic electron I/Z plotted against atomic number Z. The broken curve shows the Chu-Powers result based on a simpler and less rigorous theory.[1] The solid curve represents the present result. The chained curve represents the experimental data compiled by Andersen and Ziegler.[2]

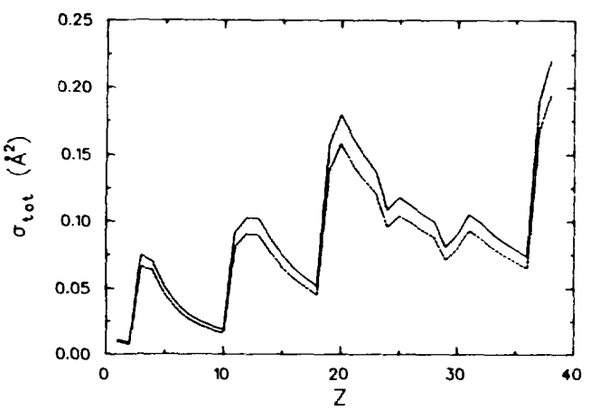

FIG. 2.--The total inelastic-scattering cross section σ_{tot} for 50-keV electrons, plotted against Z. The solid line shows the full result including relativistic-kinematic effects, while the broken line shows the result without them.

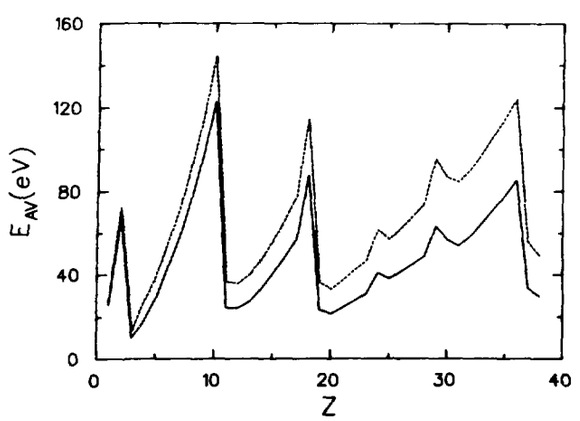

FIG. 3.--Mean energy transfer per inelastic collision of a fast charged particle, plotted against Z. The solid line applies to 50-keV electrons, while the broken line applies to the limit of high energy for any charged particle.

Finally, Figure 3 concerns the mean energy transfer per inelastic collision of a fast charged particle, i.e., a quantity decisive for radiological physics.

The present paper is a comprehensive report of work that began several years ago, resulted in three earlier papers,[3-5] and has now been technically completed. However, we have been unable to publish our entire results on the oscillator-strength distributions of thirty-eight atoms for each subshell and each channel because of the sheer volume of data. All of our results in full detail are being maintained in various forms such as computer output, microfische, magnetic tapes, or disks for reference in connection with current experimental and theoretical work. We will try to answer any reasonable inquiries about our data.

References

1. W.K. Chu and D. Powers, Phys. Lett. 40A, 23 (1972).
2. H. H. Andersen and J. F. Ziegler, The Stopping Power and Ranges of Ions in Matter, Hydrogen Stopping Powers and Ranges in All Elements, Vol. 3, Pergamon Press, New York (1977).
3. J. L. Dehmer, M. Inokuti, and R. P. Saxon, Phys. Rev. A 12, 102 (1975).
4. M. Inokuti, R. P. Saxon, and J. L. Dehmer, Int. J. Radiat. Phys. Chem. 7, 109 (1975).
5. M. Inokuti, T. Baer, and J. L. Dehmer, Phys. Rev. A 17, 1229 (1978).

BOUNDS ON MEAN EXCITATION ENERGIES IN TERMS OF OSCILLATOR-STRENGTH MOMENTS*

Isao Shimamura† and Mitio Inokuti

The logarithmic mean excitation energies that determine, for fast charged particles, the total inelastic scattering cross section, the stopping power, and the straggling are bounded from above and below by simple expressions involving moments of the oscillator-strength distribution. A general condition under which the set of elementary inequalities gives tight bounds is indicated, and is illustrated in several examples. Effective oscillator-strength distributions that are constructed on the basis of variational principles lead to tighter bounds in terms of some of the moments and the oscillator strengths for some discrete excitations.

---

*Abstract of a paper published in Phys. Rev. A 23, 2914 (1981).

†Institute of Space and Astronautical Science, Tokyo 153, Japan.

ANALYTIC REPRESENTATION OF THE DIPOLE OSCILLATOR-STRENGTH DISTRIBUTION *

Michael A. Dillon and Mitio Inokuti

It is possible to represent an essential factor of the dipole oscillator-strength distribution for a single-electron continuum in terms of a compact expression involving a polynomial of several degrees in a suitable variable. The factor, which may be called the reduced oscillator-strength distribution, is defined in terms of the radial dipole matrix element with respect to the final-state wave function normalized in an energy-independent way near the origin. The key variable is $g = \varepsilon/(\varepsilon + I)$, where ε is the kinetic energy of the ejected electron and I is the ionization threshold energy. The structure of the analytic representation has been identified through a study of the analytic properties of the dipole matrix element as a function of ε. For illustration, H, He, Li, and Na atoms are treated explicitly. Implications of our results to molecules and multichannel cases are also indicated. The present findings will be especially useful for interpolation and extrapolation of experimental data.

* Abstract of a paper published in J. Chem. Phys. 74, 6271 (1981).

ON THE FERMI-SEGRE FORMULA

Michael A. Dillon

The Fermi-Segre normalization expression is rederived for arbitrary orbital angular momentum ℓ within the context of a generalized WBK method. Results from the approximation are compared with calculations employing Hartree-Slater atomic potentials.

Introduction

The amplitude of a normalized continuum wave function at the nucleus is one of the main factors that determine the energy dependence of a photoionization cross section.[1] The same quantity in a discrete-state wave function plays an important role in the discussion of neutral currents[2] and hyperfine splitting.[3,4] In the case of s bound states, an estimate of this amplitude may be obtained from a formula first introduced by Fermi and Segre nearly fifty years ago.[5] The Fermi-Segre expression was rederived by Foldy[6] with a view to giving it a more rigorous and understandable theoretical basis. Subsequently, his treatment was extended by Bouchiat and Bouchiat[2] (hereafter referred to as BB) to include states with $\ell \neq 0$.

The method devised by Foldy was, in fact, a particular example of a general theoretical development reported a few years earlier by Miller et al.[7,8] All of the techniques mentioned here involve a variant of the WKB approximation. Thus, implementation of Miller's approach in conjunction with parallel developments[9-11] should considerably simplify the combined treatments of Foldy and BB. Also, the application of a more general but generically similar theory should provide some insight into the limitations of the WKB approach to similar problems.

Theory

Let $\Psi(r)$ be a normalized single-electron radial wave function with the usual limiting property

$$\Psi \sim C\, r^{\ell} + \ldots \,, \tag{1}$$

where r is the radial coordinate. The point of this discussion is to find an approximate form for C^2 in terms of the energy W, angular momentum number ℓ, and the atomic number Z. We begin with the unnormalized wave function, ψ, defined through the reduced radial function P(r) by

$$P = r\psi \quad . \tag{2}$$

P is the solution of the ordinary differential equation

$$d^2P/dr^2 + f^2 P = 0 \quad , \tag{3}$$

where

$$f^2 = 2W - V - L^2/r^2 \quad , \tag{4}$$

and $\ell(\ell + 1) = L^2$. Here atomic units are used. The potential V possesses the properties

$$V \to -2Z/r \quad \text{as } r \to 0 \; ; \qquad V \to -2/r \quad \text{as } r \to \infty \quad . \tag{5}$$

We wish to approximate ψ by applying a kind of asymptotic perturbation theory known as the generalized WKB method.[7,8] In the ordinary WKB approach, P is approximated by a product function

$$P \cong T(r)\ \phi(S) \quad , \tag{6}$$

where $S = S(r)$, $\phi = \exp[\pm i(2W)^{1/2}S]$ and $T = S'^{-1/2}$. Of course, the exponential function itself is a solution of the differential equation

$$d^2\phi/dS^2 - F^2\phi = 0 \quad , \tag{7}$$

with $F^2 = 2W$. An obvious generalization of the WKB method is to extend the definition of F^2 in Eq. 7 to

$$F^2 = 2E - U - L^2/S^2 \quad , \tag{8}$$

and at the same time retain the ansatz 6. Ultimately we shall be concerned with the bound states of Eqs. 3 and 7. However, W and E in Eqs. 4 and 8 are to remain continuous unless otherwise specified as subscripted quantities.

Inserting Eq. 6 into Eq. 3 and using Eqs. 7 and 8, we get

$$(T''/T - S'^{1/2}F^2 + f^2)T\phi + (2T'/T + S''/S')TS'\, d\phi/dS = 0 \quad . \tag{9}$$

Then, in the spirit of the WKB method, let

$$T = S'^{-1/2} \quad , \tag{10}$$

and Eq. 9 becomes

$$T''/T - S^{1/2} F^2 + f^2 = 0 \quad . \tag{11}$$

As the first step of an interative solution of Eq. 11, $T''/T \sim 0$ and

$$S' = f/F \quad . \tag{12}$$

Equation 12 gives S to zeroth order; therefore to zeroth order,

$$P \cong (F/f)^{1/2} \phi(S) = S'^{-1/2} \phi(S) \quad . \tag{13}$$

Since $P \to O(r^{\ell+1})$ as $r \to 0$, it will be convenient to choose U in Eq. 8 so that

$$\phi(S) \to O(S^{\ell+1}) \qquad \text{as } S \to 0 \quad . \tag{14}$$

This limit imposes a further condition on $S(r)$, namely

$$S(r) \to A_\ell \cdot r \qquad \text{as } r \to 0 \quad . \tag{15}$$

Then, Eqs. 4, 8, 14, and 15 show that the approximate P given by Eq. 13 approaches $O(r^{\ell+1})$ at small r. Specifically,

$$P \to (A_\ell)^{\ell+1/2} r^{\ell+1} \qquad \text{as } r \to 0 \quad , \tag{16}$$

which is the required form.

Unlike WKB-type wave functions, P of Eq. 13 can be made continuous across the classical turning points. Let r_1, r_2, S_1, and S_2 be the inner and outer turning points of the respective radial equations 3 and 7. Then impose the conditions

$$S(r_1) = S_1 \qquad \text{and} \qquad S(r_2) = S_2 \quad . \tag{17}$$

In any realistic application of this approximation, f and F in Eq. 12 will have zeros of the same order at r_1 and S_1, respectively. Hence, in contrast to the ordinary WKB method, T in Eq. 6 will be continuous at the classical turning points in Eq. 3.

Equation 12 may be rewritten

$$\int F \, dS = \int f \, dr \quad . \tag{18}$$

Then explicit application of conditions 17 give for the region $0 \leq r \leq r_1$, $0 \leq S \leq S_1$,

$$\int_0^{S_1} [2EX^2 - 2UX^2 - L^2]^{1/2} X^{-1}\, dX = \int_0^{r_1} [2WX^2 - 2VX^2 - L^2]^{1/2} X^{-1}\, dX \tag{19}$$

and for the region between the turning points,

$$\int_{S_1}^{S_2} [2EX^2 - 2UX^2 - L^2]^{1/2} X^{-1}\, dX = \int_{r_1}^{r_2} [2WX^2 - 2VX^2 - L^2]^{1/2} X^{-1}\, dX \ . \tag{20}$$

It will be shown that Eq. 19 suffices to determine A. It is also clear that Eq. 20 determines the approximate eigenenergy W_n in terms of E_n. With both quantities A_ℓ and W_n known, numerical integration of Eq. 12 becomes a simple matter.

We need to examine briefly certain normalization properties of P and ϕ.[7,11] For arbitrary (negative) W in Eq. 3, there exists an independent pair of solutions P_1 and P_2 with the following properties:

$$P_1 \to O(r^{\ell+1}) \quad \text{as } r \to 0\,, \qquad P_1 \to \infty \text{ as } r \to \infty \tag{21a}$$

$$P_2 \to O(r^{-\ell}) \quad \text{as } r \to 0\,, \qquad P_2 \to 0 \text{ as } r \to \infty\ . \tag{21b}$$

The two functions become equivalent at the eigenenergies. That is

$$P_1 = P_2 = P_n, \quad \text{when } W = W_n\ .$$

Yngve,[11] improving on an earlier result by Furry,[9] has shown that

$$\int_0^\infty P_n^{\,2}\, dr = N^{-2} = \frac{d}{dW}\,(P_1P_2' - P_2P_1')\ \Big|_{W = W_n}\ . \tag{22}$$

Of course, since ϕ_n is also an eigenfunction, it must be true that

$$\int_0^\infty \phi_n^{\,2}\, dS = N_0^{-2} = \frac{d}{dE}\,(\phi_1\phi_2' - \phi_2\phi_1')\ \Big|_{E = E_n}\ . \tag{23}$$

We note that

$$\frac{dP_1}{dr} \cong \frac{d\, S'^{-1/2}\phi_1}{dr} = S'^{1/2}\frac{d\phi_1}{dS} - \tfrac{1}{2}\phi\, S''S'\ ,$$

and substitute the required forms into Eq. 22 with an obvious change of variable; the P normalization becomes

$$N^{-2} = \frac{dE}{dW} \frac{d}{dE} (\phi_1 \phi_2' - \phi_2 \phi_1') \Big|_{W=W_n} . \tag{24}$$

Equations 23 and 24, together with the fact that $W = W_n$ when $E = E_n$, provide an approximate form for N^2,

$$N^2 \cong N_0^{\,2} \frac{dW}{dE} \Big|_{E=E_n} . \tag{25}$$

Finally, we obtain C^2 from Eqs. 1, 2, 16, and 25

$$C^2 = \left(\frac{N P(0)}{r^{\ell+1}} \right)^2 \cong N_0^{\,2} \frac{dW}{dE} \Big|_{E=E_n} (A_\ell)^{2\ell+1} . \tag{26}$$

With the derivation of Eq. 26, the problem is practically solved. There remains the relatively simple task of employing the usual hydrogenic models to find A. Thus, we may put

$$U = 2\bar{Z}/S \tag{27}$$

in Eq. 8, and rewrite V in Eq. 4 as

$$V = -(2Z/r)\, \eta(r) . \tag{28}$$

In Eq. 27, $\bar{Z} = 1$ and $\bar{Z} = Z$ tests the two obvious possibilities. Then with U given by Eq. 27, we have for E_n

$$E_n = -\bar{Z}^2/(2n^2) = \bar{Z}^2 E_{cn} \tag{29}$$

and for $N_0^{\,2}$,

$$N_0^{\,2} = \left[\frac{2^{\ell+1}}{(2\ell+1)!} \right]^2 \frac{(n+\ell)!}{(n-\ell-1)!} \frac{\bar{Z}^{2\ell+3}}{n^{2\ell+4}} = N_c^{\,2} \bar{Z}^{2\ell+3} . \tag{30}$$

Equation 26 becomes

$$C^2 = N_c^{\,2} \bar{Z}^{\,2\ell+1} \frac{dW}{dE_c} \Big|_{E=E_{nc}} (A_\ell)^{2\ell+1} , \tag{31}$$

where the subscript c refers to the corresponding hydrogenic parameters. The derivative in Eq. 31 may be written in a more familiar way,

$$\left.\frac{dW}{dE}_c\right|_{E=E_{cn}} = n^3 \frac{dW}{dn} \quad . \tag{32}$$

Also, when n is large,

$$N_c^2 \to \left[\frac{2^{\ell+1}}{(2\ell+1)!}\right]^2 n^{-3} \qquad \text{so that}$$

$$C^2 \to \left[\frac{2^{\ell+1}}{(2\ell+1)!}\right]^2 \bar{Z}^{2\ell+1} \frac{dW}{dn} (A_\ell)^{2\ell+1} \quad \text{as } n \to \infty \quad . \tag{33}$$

Equation 31 is now in the exact form reported by Iwinski et al.[12,13] They continue by calculating A within the framework of an analytical perturbation theory. The present method employs Eq. 19 written in the form of the limit

$$\int_{S=Ar}^{S_1} [2E_n X^2 - 2\bar{Z}X - L^2]^{1/2} X^{-1} dX - \int_r^{r_1} [2W_n X^2 - 2Z\eta X - L^2]^{1/2} X^{-1} dX \to 0$$

as $r \to 0$, which may be shown to give

$$\ln A = (2L^2E_{cn})^{-1/2} \ln \frac{[1 - (2L^2E_{cn})^{1/2}]}{(1 - 2L^2E_{cn})^{1/2}} + \ln \frac{2L^2/r_1}{\bar{Z}(1 - 2L^2E_{cn})^{1/2}} - 1$$

$$+ \int_0^{r_1} \{1 - [1 - \frac{2Z\eta}{L^2} X + \frac{2W_n}{L^2} X^2]^{1/2}\} X^{-1} dX \quad . \tag{34}$$

An important consequence of Eq. 34 is that C^2 is independent of $\bar{Z}$. Hence, it makes no difference whether one uses U = 1/2S or U = Z/S as a reference potential in Eq. 8. At the ionization limit $W_n = E_{cn} = 0$ and Eq. 34 becomes

$$\ln A_\ell = \ln(2L/\bar{Z}r_1) - 2 + \int_0^{r_1} \{1 - [1 - \frac{2Z\eta}{L^2}]^{1/2}\} X^{-1} dX \quad . \tag{35}$$

When $L^2 = 0$, then $r_1 = S_1 = 0$ and W_n is still obtained from the integral relationship Eq. 20. However, the region $0 \leq S \leq S_1$, $0 \leq r \leq r_1$ no longer exist and Eq. 19 is unavailable for the evaluation of A. However, it must be true that Eq. 18 in the form

$$\int_0^S [2E_n X^2 + 2\bar{Z}X]^{1/2} X^{-1} dX = \int_0^r [2W_n X^2 + 2Z\eta X]^{1/2} X^{-1} dX \qquad (36)$$

holds for small r and S. In the present calculation, $2Z\eta/r$ is a Hartree-Slater potential (HS) and η has the form (cf. Eq. 5)

$$\eta = 1 + \sum_{k=1}^{k=\infty} n_k r^k \quad . \qquad (37)$$

When S and r are small, Eq. 36 becomes

$$(2\bar{Z})^{1/2} \int_0^{s=A_\ell r} X^{-1/2} dX \; (2Z)^{1/2} \int_0^r X^{-1/2} dX \quad , \qquad (38)$$

from which we get $A_0 = 1$ when $\bar{Z} = Z$ and $A = Z$ when $\bar{Z} = 1$. These two forms for A_0 lead to the same result. In fact, in Eqs. 31 and 33, both expressions for C^2 are alternative versions of the Fermi-Segre formula. Once again, C^2 is independent of whether $U = 2/S$ or $U = 2Z/S$ is used in Eq. 8. However, the most remarkable feature of this result is the independence of A_0 with respect to the η_k. Thus, it would appear that the most general type of WKB formulation for $\ell = 0$ succeeds in reproducing the original Fermi-Segre expression.

We wish to compare calculated values of the parameter[3]

$$M_\ell = \left[\frac{C(2\ell + 1)!}{Z^{\ell+\frac{1}{2}} S^{\ell+1}} \right]^2 \qquad (39)$$

for zero energy continuum wave functions with the limiting form given in Eq. 33. It is known that such a procedure involves the removal[3] of the factor $dW/d\eta$ from Eq. 33 so that

$$M_\ell \equiv (A_\ell)^{2\ell + 1} \quad . \qquad (40)$$

Thus, for the original Fermi-Segre case, we have $M_0 = 1$. In Figure 1 this result is compared to values of M_0 for the interval Z = 1 to 36 calculated by direct integration of Eq. 3 using HS potentials* from the compilation of Herman-Skillman.[14] The plots in the figure show that $M_0 = 1$ reproduces the average calculated M_0 fairly well. However, the effects of periodicity, as well as individual atomic

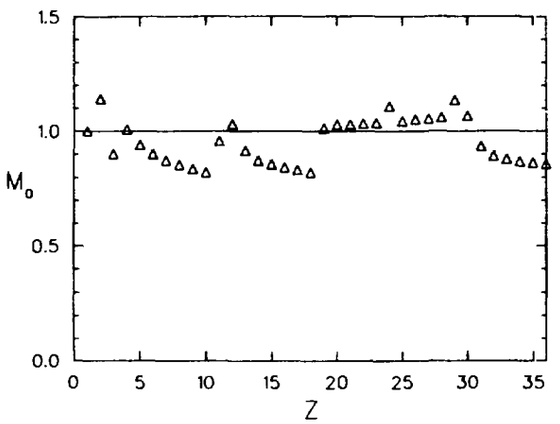

FIG. 1.--A plot M_0 vs. Z at W =2. —, Fermi-Segre formula with A_0 =1; Δ, calculated data points using HS atomic potentials.

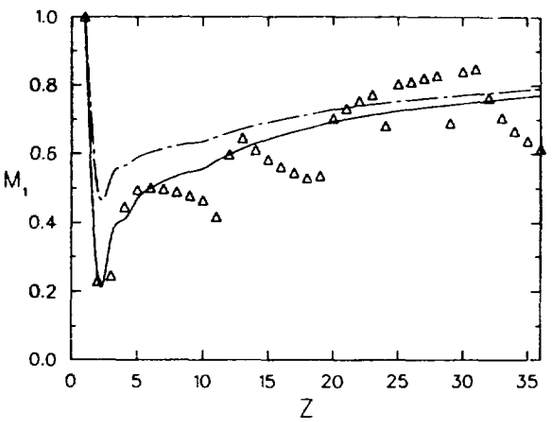

FIG. 2.--A plot of M_1 vs. Z at W =0. —, Fermi-Segre formula from Eq. 41; Δ, calculated data points using HS atomic potentials.

variations, are clearly missing. This discrepancy must be a shortcoming of a WKB type of approximation since $M_0 = 1$ is the best we can do within the framework of the present theory.

In order to compare our results with those of BB, we integrate Eq. 35 by assuming a linear form for Eq. 37. This gives

$$\ln A_\ell = \frac{1}{\sigma^{1/2}} \ln \frac{(1-\sigma)^{1/2}}{(1-\sigma^{1/2})} + \ln(1-\sigma)^{1/2} - 1 \qquad (41)$$

with

$$\sigma = 2\eta_1/L^2 \ .$$

---

*Both the integration code and the HS data sets were kindly provided by J. L. Dehmer. The numerical calculations presented here may be found in Ref. 3.

The amplitude $(A_\ell)^{2\ell+1}$ obtained from Eq. 41 may be expanded to first order in σ to yield

$$(A_\ell)^{2\ell+1} \cong -(2\ell + 1)\ \ell\ (\ell + 1)\ \eta_1/3 \quad . \tag{42}$$

This form of $(A_\ell)^{2\ell+1}$ is identical to the result of BB for $W_n = 0$. In Figure 2, $M_1 = (A_1)^3$ from both Eqs. 41 and 42 are compared with values of M_1 derived from the integration[15] of Eq. 3 employing HS potentials. The parameters η_1 used in σ of Eq. 41 were computed from the same potentials. Again, the effects of periodicity observed in the computed points are missing from approximations (Eqs. 41 and 42). The approximate curves, especially the one intengrated by Eq. 41, smoothly follow the calculated points. The structure in the calculated points clearly follows from the full utilization of the HS potentials in the integration of Eq. 3. In contrast, the approximate M_1 uses only η_1 of Eq. 37, while M_0 is entirely independent of the model potential.

References

1 M. A. Dillon and M. Inokuti, J. Chem. Phys., in press.
2. M. A. Bouchiat and C. Bouchiat, J. Phys. 35, 899 (1974).
3. U. Fano, C. E. Theodosiou, and J. L. Dehmer, Rev. Mod. Phys. 48, 49 (1976).
4. M. F. Crawford and A. L. Schawlow, Phys. Rev. 76, 1310 (1949).
5. E. Fermi and E. Segre, Z. Physik 82, 729 (1933).
6. L. L. Foldy, Phys. Rev. 111, 1093 (1958).
7. S. C. Miller, Jr. and R. G. Good, Jr., Phys. Rev. 91, 174 (1953).
8. S. C. Miller, Jr., Phys. Rev. 94, 1345 (1954).
9. W. H. Furry, Phys. Rev. 71, 360 (1947).
10. N. Fröman and P. O. Fröman, Phys. Rev. A 6, 2064 (1972).
11. S. Yngve, J. Math. Phys. 13, 324 (1972).
12. Z. R. Iwinski, Y. S. Kim, and R. H. Pratt, Phys. C 19, 1924 (1979).
13. Z. R. Iwinski, Y. S. Kim, and R. H. Pratt, Phys. Rev. A 22, 1358 (1980).
14. F. Herman and S. Skillman, Atomic Structure Calculations (Prentice-Hall, Englewood Cliffs, N. J., 1963).
15. J. L. Dehmer, Radiological and Environmental Research Division, private communication (1980).

THE FUTURE OF THEORETICAL ATOMIC-COLLISION PHYSICS*

Mitio Inokuti

Several important issues must be resolved for the establishment of an eventual theory of inelastic collisions of electrons with atoms and molecules; some of the issues are also relevant to collisions between atoms or molecules. Some lines of approach that are likely to contribute to substantial progress are suggested.

*Summary of an article published in Comments At. Mol. Phys. 10, 99 (1981).

RELATIVISTIC BORN CROSS SECTIONS FOR THE ELECTRON IMPACT EXCITATION*

Yong-Ki Kim

Relativistic effects in electron-atom collisions have three origins: (a) From atomic structure (intermediate coupling, changes in orbital sizes, etc.); this effect is important in heavy atoms. (b) From relativistic kinematics (correct energy-momentum formulas); this is important for fast incident electrons. (c) From relativistic interactions (transverse virtual photon); this is also important for fast incident electrons.

To understand the relative significance of these effects, Born cross sections for electron-impact excitations of Li-like gold ion, Au^{76+}, were calculated both in relativistic and nonrelativistic forms.

The relativistic Born cross section for the excitation from the initial state $|0)$ to an excited state $|n)$ is[1]

$$\frac{d\sigma_n}{dQ} = \frac{4\pi a_0^{\,2}\alpha^2}{\beta^2}\left\{\frac{|F_n(K)|^2}{Q^2} + \frac{|\vec{\beta}_t \cdot \vec{G}_n(K)|^2}{[Q-(\alpha E_n/2R)^2]^2}\right\} \quad . \tag{1}$$

where $\alpha = 1/137$, $a_0 = 0.529\mathring{A}$, $R = 13.6$ eV, E_n is the excitation energy, $Q = (Ka_0)^2$ with momentum transfer $\hbar\vec{K}$, $\vec{\beta} = \vec{v}/c$ with incident electron velocity $\vec{v}$, and $\vec{\beta}_t$ is the component of $\vec{\beta}$ perpendicular to $\vec{K}$. The form factors $F_n(K)$ and $G_n(K)$ are defined as[1]

$$F_n(K) = \sum_j (n|e^{i\vec{K}\cdot\vec{r}_j}|0) \quad , \tag{2}$$

and

$$\vec{G}_n(K) = \sum_j (n|\vec{\alpha}_j e^{i\vec{K}\cdot\vec{r}_j}|0) \quad , \tag{3}$$

where the summation is over all bound electrons, $\vec{r}_j$ is the position vector of

---

*Summary of a paper presented at the 7th Int. Conf. on Atomic Physics held at Massachusetts Institute of Technology, August 4-8, 1980.

the jth electron, and $\vec{\alpha}$ is the Dirac matrix. The form factor $F_n(K)$ represents the longitudinal (nonrelativistic Coulomb) interaction, and $\vec{G}_n(K)$ the transverse interaction (equivalent to the Breit interaction). In the nonrelativistic Born formula, only $F_n(K)$ appears.

In an earlier analysis, Fano showed[2] that the transverse interaction peaks sharply at very small angles. He also showed that the integrated cross section for the excitations,

$$\sigma_n = \int (d\sigma_n/dQ)dQ \quad ,$$

should have the form (commonly known as the Bethe formula[3])

$$\sigma_n = 4\pi a_0^2 \alpha^2 \beta^{-2} (A_n\{\ln[\beta^2/(1-\beta^2)] - \beta^2\} + B_n) \quad , \tag{4}$$

where constants A_n and B_n depend only on the properties of the targe.

In Figures 1-3, we compare σ_n calculated in four different ways; (i) with nonrelativistic formula (i.e., only with $F_n(K)$ and nonrelativistic wave functions), (ii) with relativistic longitudinal interaction only (i.e., only with $F_n(K)$ but with relativistic wave functions), (iii) with relativistic longitudinal and transverse interactions (i.e., with $F_n(K)$, $\vec{G}_n(K)$ and relativistic wave functions), and finally with the Bethe formula, Eq. 4, where A_n and B_n are determined from relativistic wave functions. The difference A results from the relativistic atomic structure as embodied in the relativistic wave functions. The difference B originates from the kinematics, the difference between relativistic and nonrelativistic kinematics. The difference C represents the contribution from the transverse interaction.

From Figures 1-3, we conclude as follows:

(a) The relativistic atomic structure and kinematics are important in both allowed and forbidden transitions. One must use relativistic formulas and wave functions. (b) The transverse interaction is significant only for allowed transitions and very fast incident electrons ($\beta^2 > 0.9$). (c) The Bethe formula for the integrated cross section (Eq. 4) agrees well with the correct Born cross sections for fast electrons. The Bethe parameters, however, must be computed from the relativistic wave functions of the target.

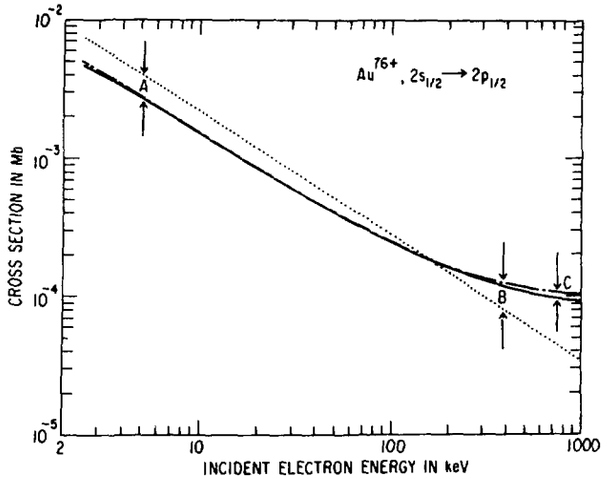

FIG. 1.--Cross section for the $2s_{1/2}$ - $2p_{1/2}$ excitation of Au^{76+} by electron impact (i) Nonrelativistic formula and wave functions, ...; (ii) Longitudinal interaction only with relativistic wave functions, ——;(iii) Longitudinal and transverse interactions with relativistic wave functions, ----; (iv) The Bethe formula with relativistic wave functions, -.-.-.-. See the text for the explanation of A, B, and C.

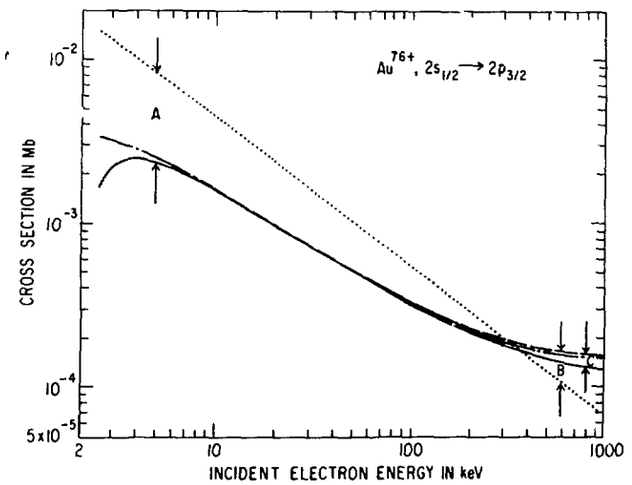

FIG. 2.--Cross section for the $2s_{1/2}$ - $2p_{3/2}$ excitation of Au^{76+} by electron impact. Symbols as in Figure 1.

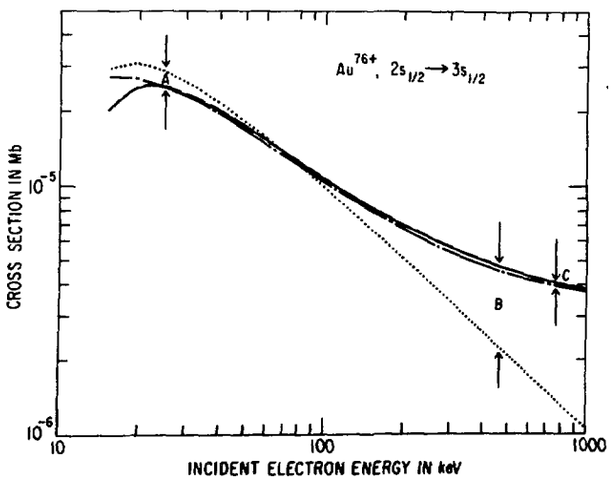

FIG 13.--Cross section for the $2s_{1/2}$ - $3s_{1/2}$ excitation of Au^{76+} by electron impact. Symbols as in Figure 1.

References

1. U. Fano, Ann. Rev. Nucl. Sci. 13, 1 (1963).
2. U. Fano, Phys. Rev. 102, 385 (1956).
3. H. A. Bethe, in Handbuch der Physik, Vol. 24/1, Springer, Berlin (1933).

TRANSITION PROBABILITIES FOR ATOMS*

Yong-Ki Kim

The current status of advanced theoretical methods for transition probabilities for atoms and ions is summarized in Table 1. An experiment on the f values of the resonance transitions of the Kr and Xe isoelectronic sequences is suggested as a test for the theoretical results.

Table 1. Current Status of Advanced Theories for Transition Probabilities

	MCHF[a]	RPA[b]	MBPT[c]
Open shell	Yes	Not yet	Yes, in principle
Relativity	Yes	Yes	Not yet
Continuum correlation	Indirect, difficult	Direct, RPA equation	Direct, brute force
Gauge invariance	No	Yes	Depends
Accuracy	Good	Better	Best, in principle
Isoelectronic sequences	Yes	Yes, but limited	Not yet

[a]Multiconfiguration Hartree-Fock method.

[b]Random phase approximation.

[c]Many-body perturbation theory.

*Summary of an invited talk presented at the Workshop on Atomic Physics at the National Synchrotron Light Source, Brookhaven National Laboratory, September 15-17, 1980, Report No. BNL-28832, pp. 33-41.

REPORT ON THE WORKSHOP ON ATOMIC AND PLASMA PHYSICS REQUIREMENTS FOR HEAVY ION FUSION, ARGONNE NATIONAL LABORATORY, DECEMBER 13-14, 1979*

Yong-Ki Kim

The workshop, which was organized by Y.-K. Kim and G. R. Maggelssen (ANL Accelerator Research Facilities Division), identified atomic, molecular, and plasma physics areas relevant to intertial confinement fusion by energetic heavy ions. Discussions were confined to problems related to the design of heavy ion accelerators, accumulation of ions in storage rings, and the beam transport in a reactor vessell. The atomic and molecular data needed are listed in Table 1 with recommended priorities.

Table 1. Atomic and molecular data relevant to heavy-ion fusion. Priorities depend very much on the accelerator and reactor pressure under consideration.

Type of data	Where they are needed	Priority	Preferred method
Ion-gas charge-changing cross-section ($< 10^9$ cm/sec)	Induction Linac	Primary	Experiment
Ion-gas stripping cross-sections ($> 10^9$ cm/sec)	re linac, synchrotron (storage ring)	Secondary	Theory
Ion-ion charge-changing cross sections ($< 10^8$ cm/sec)	rf linac synchrotron (storage ring)	Primary	Experiment
Charge states ($< 10^{-3}$ Torr)	Reactor	Primary	Theory with benchmark experiment
Charge states (10^{-3} - 10 Torr)	Reactor	Secondary	Theory with benchmark experiment
Secondary-electron distribution	Reactor	Secondary	Experiment
Electron degradation	Reactor	Secondary	Theory
Plasma diagnostics	Reactor	Secondary	Experiment

*Summary of Argonne National Laboratory Report ANL-80-17 (available from the National Technical Information Service, U.S. Dept. of Commerce, Springfield, Va. 22161).

PUBLICATIONS BY THE STAFF OF THE FUNDAMENTAL MOLECULAR PHYSICS AND CHEMISTRY SECTION FOR THE PERIOD OCTOBER 1979-SEPTEMBER 1980.

MAJOR PAPERS

K. T. Cheng, Y.-K. Kim, and J. P. Desclaux, Electric dipole, quadrupole, and magnetic dipole transition probabilities of ions isoelectronic to the first-row atoms, Li through F, Atomic Data and Nuclear Tables 24(2), 111 (1979).

B. E. Cole, D. L. Ederer, R. Stockbauer, K. Codling, A. C. Parr, J. B. West, E. D. Poliakoff, and J. L. Dehmer, Wavelength and vibrational-state dependence of photoelectron angular distribution. Resonance effects in 5σ photoionization of CO, J. Chem. Phys. 72, 6308 (1980).

J. L. Dehmer, Jon Siegel, J. Welch, and Dan Dill, Origin of enhanced vibrational excitation in N_2 by electron impact in the 15-35 eV region, Phys. Rev. A 21(1), 101-104 (1980).

P. M. Dehmer and W. A. Chupka, Predissociation of the $3p\pi\ ^1\Pi_u$ state in H_2, HD, and D_2, Chem. Phys. Letters 70(1), 127-130 (February 1980).

P. M. Dehmer, J. L. Dehmer, and W. A. Chupka, Effect of vibronic interaction and autoionization on the photoelectron spectrum of N_2O, J. Chem. Phys. 73(1), 126-133 (July 1980).

J. P. Desclaux, K. T. Cheng, and Y.-K. Kim, Relativistic energy levels of Fe XXI, J. Phys. B: Atom. Molec. Phys. 12(23), 3819-3825 (December 1979).

D. Dill, J. Welch, J. L. Dehmer, and J. Siegel, Shape-resonance-enhanced vibrational excitation at intermediate energies (10-40 eV) in electron-molecule scattering, Phys. Rev. Lett. 43, 1236 (1979).

E. Eggarter and Mitio Inokuti, Cross sections for electron inelastic collisions with argon, ANL-80-58 (July 1980).

K. N. Huang, W. R. Johnson, and K. T. Cheng, Totally polarized electrons from photoionization of outer $p_{1/2}$ subshells of rare gases: A relativistic random phase approximation calculation, Phys. Letters 77A(4), 234-236 (May 1980).

Mitio Inokuti, Atomic processes pertinent to radiation physics, Electronic and Atomic Collisions, Eds., N. Oda and K. Takayanagi (North-Holland Publ. Co., 1980), pp. 31-45.

Mitio Inokuti, Disturbing the Universe, by Freeman Dyson. (Book review), Proc. Phys. Soc. Japan 35, 541 (June 1980) (in Japanese).

M. Inokuti, H. Sekine, and T. Mura, General use of the Lagrange multiplier in nonlinear mathematical physics, in Variational Methods in the Mechanics of Solids. Proceedings of the IUTAM Symposium on Variational Methods in the Mechanics of Solids, 11-13 September 1978, Evanston, Illinois, edited by S. Nemet-Nasser (Pergamon, London, 1980), pp. 156-162.

Mitio Inokuti, Atomic and Molecular Collisions, by Sir Harrie Massey (Book Review), American Scientist 68, 320 (May-June 1980).

Mitio Inokuti, On the evaluation of the Born partial-wave amplitude for electron scattering by an electrostatic multipole field, J. Phys. B: Atom. Molec. Phys. 13, 1221-1227 (March 1980).

Mitio Inokuti, D. A. Douthat, and A.R.P. Rau, Statistical fluctuations in the ionization yield and their relation to the electron degradation spectrum, Phys. Rev. A 22(2), 445-453 (August 1980).

Yong-Ki Kim and Kwok-tsang Cheng, Stopping power for partially stripped ions, Phys. Rev. A 22(1), 61-67 (July 1980).

Maureen G. Lynch, Dan Dill, Jon Siegel, and J. L. Dehmer, Elastic electron scattering by CO_2, OCS, and CS_2 from 0 to 100 eV, J. Chem. Phys. 71(11), 4249-4254 (December 1979).

S. T. Manson and M. Inokuti, Near-threshold structure in the atomic K-shell spectra for ionization by photons or by fast charged particles, J. Phys. B: Atom. Molec. Phys. 13, L323-L326 (May 1980).

P. P. Nicole, Removal of volatile materials from forepump oil, J. Vac. Sci. Technol. 17, 1384 (1980).

A. C. Parr, Roger Stockbauer, B. E. Cole, D. L. Ederer, J. L. Dehmer, and J. B. West, An angle resolved photoelectron spectrometer for atoms and molecules, Nucl. Instrum. Methods 172, 357-361 (May 1980).

J. C. Person and P. P. Nicole, Interface for rapid data transfer from NIM counters to small computers, Rev. Sci. Instrum. 51, 1425-1426 (1980).

E. Shiles, Taizo Sasaki, Mitio Inokuti, and D. Y. Smith, Self-consistency and sum-rule tests in the Kramers-Kronig analysis of optical data: Application to aluminum, Phys. Rev. B 22(4), 1612-1628 (August 1980).

Jon Siegel, J. L. Dehmer, and Dan Dill, Differential cross sections for e-LiF scattering, J. Phys. B: Atom. Molec. Phys. 13, L215-L219 (1980).

Jon Siegel, J. L. Dehmer, and Dan Dill, Elastic-electron-scattering cross sections for N_2 from 0 to 1000 eV. Energy-dependent exchange potentials, Phys. Rev. A 21(1), 85-94 (January 1980).

David Spence, A technique to enhance and separate negative ions from neutral autoionising features in scattered electron spectra in the ionisation continuum: Application to negative ions in neon, J. Phys. B: Atom. Molec. Phys. 13, 1611-1624 (1980).

David Spence and P. D. Burrow, Cross sections for excitation of the $2s^2 2p^2 3s\ ^4P$ and $(2s2p^4)\ ^4P$ states of atomic nitrogen by near-threshold electron impact, J. Phys. B: Atom. Molec. Phys. 13, 2809-2815 (1980).

David Spence, Measurements of the ratio of the He $2^1S/2^3S$ energy-integrated total cross sections from threshold to 0.10 eV. Comparison with theory, J. Phys. B: Atom. Molec. Phys. 13, L73-L77 (1980).

J. R. Swanson, D. Dill, and J. L. Dehmer, Nuclear motion effects in the photoionization of CO_2, J. Phys. B 13, L231 (1980).

J. B. West, A. C. Parr, B. E. Cole, D. L. Ederer, R. Stockbauer, and J. L. Dehmer, Shape-resonance-induced non-Franck-Condon vibrational intensities in $3\sigma_g$ photoionization of N_2, J. Phys. B: Atom. Molec. Phys. 13(3), L105-L108 (February 1980).

CONFERENCE PAPERS AND ABSTRACTS

XIth Annual Meeting of the Division of Electron and Atomic Physics, the American Physical Society, Houston, Texas, 10-12 December 1979. Bull. Am. Phys. Soc. 24(9) (November 1979).

P. M. Dehmer and P. S. Dardi, Predissociation decay rates for selected vibrational levels of the $3p\pi\ ^1\Pi_u$ state in H_2, HD, and D_2, p. 1191.

P. M. Dehmer and P. S. Dardi, High-resolution study of photoabsorption and photoionization in HD and D_2, p. 1201.

S. T. Manson and M. Inokuti, Generalized oscillator strength for ionization of the K and L shells of atoms. II, p. 1171.

J. L. Dehmer (invited paper), Interaction of electronic and vibrational motion in molecular photoionization. Recent experiments and theory, p. 1188.

J. Siegel, J. L. Dehmer, and D. Dill, Hybrid calculation of e-LiF scattering, p. 1170.

1980 Annual Meeting of the American Physical Society, January 21-24, 1980, Chicago. Bull. Am. Phys. Soc. 25(1) (January 1980).

M. Inokuti and D. A. Douthat, Statistical fluctuations in the ionization yield upon electron degradation of gases, p. 37.

A. C. Parr, R. Stockbauer, J. L. Dehmer, B. E. Cole, D. L. Ederer, and J. B. West, Triply-differential photoionization studies of small molecules, Book of abstracts, 28th Annual Conference on Mass Spectrometry and Allied Topics, 25-30 May 1980, New York, New York.

VI International Conference on Vacuum Ultraviolet Radiation Physics, 2-6 June 1980, University of Virginia, Charlottesville, Virginia. Abstracts appear in Book of Extended Abstracts.

E. D. Poliakoff, J. L. Dehmer, A. C. Parr, D. Dill, K. H. Jackson, and R. N. Zare, Polarized fluorescence excitation spectroscopy of N_2, II-25.

S. Wallace, J. R. Swanson, D. Dill, and J. L. Dehmer, Molecular photoelectron branching ratios and angular distributions from 0 to 10 Ry. Effects of shape resonances and vibration, II-13.

K. Codling, J. B. West, A. C. Parr, J. L. Dehmer, B. E. Cole, D. L. Ederer, and R. Stockbauer, Partial cross sections, vibrational branching ratios, and angular distributions in the 570-600 Å window resonances in O_2, II-14.

A. C. Parr, J. L. Dehmer, B. E. Cole, D. L. Ederer, R. L. Stockbauer, and J. B. West, An angle-resolved photoelectron spectrometer for triply-differential photoionization studies, III-70.

J. L. Dehmer, A. C. Parr, J. B. West, K. Codling, D. L. Ederer, B. E. Cole, E. D. Poliakoff, and R. Stockbauer, Effects of shape resonances on vibrational branching ratios and photoelectron angular distributions in molecular photoionization, II-86.

R. Stockbauer, A. C. Parr, J. L. Dehmer, B. E. Cole, D. L. Ederer, J. B. West, and K. Codling, Perturbation of vibrational intensity and angular distributions by autoionization in molecular photoionization, II-15.

J. C. Person and P. P. Nicole, Microcomputer control of absorption experiments, III-31.

J. C. Person, P. P. Nicole, and D. E. Fowler, Absorption cross sections of the chloromethanes from threshold to 21 eV, II-79.

VIIth International Conference on Atomic Physics, Massachusetts Institute of Technology, August 4-8, 1980. Book of Abstracts.

Yong-Ki Kim, Relativistic Born cross sections for the electron impact excitation, p. 111.

W. R. Johnson, K. T. Cheng, K.-N. Huang, and M. le Dourneuf, Analysis of Beutler-Fano autoionizing resonances in the rare gas atoms using the relativistic multichannel quantum defect theory, p. 68.

K.-N. Huang, W. R. Johnson, and K. T. Cheng, Angular distribution and spin polarization of photoelectrons from noble gases, p. 182.

Molecular Spectroscopy and Dynamics with Synchrotron Radiation — A European Workshop, 28 September-1 October 1980, Maria Laach, West Germany. Book of Abstracts:

J. L. Dehmer and D. Dill, Shape resonances in molecular photoionization (Invited talk), pp. 43-45.

K. Codling, J. B. West, A. C. Parr, J. L. Dehmer, and R. L. Stockbauer, Photoelectron angular distribution measurements through autoionizing resonances in argon and xenon, pp. 52-54.